δ2H of water from fluid inclusions in Proterozoic halite: Evidence for a deuterium-depleted hydrosphere?

Christophe Lécuyer, François Fourel, Nigel Blamey, Uwe Brand, Philip Fralick

δ^2H of water from fluid inclusions in Proterozoic halite: Evidence for a deuterium-depleted hydrosphere?

Christophe Lécuyer[1], François Fourel[2], Nigel Blamey[3], Uwe Brand[4], Philip Fralick[5]

[1]Laboratoire de Géologie de Lyon, UMR CNRS 5276, University of Lyon and Institut Universitaire de France, 69622, France. clecuyer@univ-lyon1.fr

[2]Laboratoire d'Ecologie des Hydrosystèmes Naturels et Anthropisés LEHNA, UMR CNRS 5023, University of Lyon, France. francois.fourel@univ-lyon1.fr

[3]Department of Earth Sciences, University of Western Ontario, London, N6A 5B7, ON, Canada. nblamey2@uwo.ca

[4]Department of Earth Sciences, Brock University, 1812 Sir Isaac Brock Way, St Catharines, ON L2S 3A1, Canada. ubrand@brocku.ca

[5]Department of Geology, Lakehead University, Thunder Bay, ON P7B 5E1, Canada. pfralick@lakeheadu.ca

Keywords: Proterozoic; water cycle; ^{2}H/^{1}H ratio; halite; fluid inclusion

Abstract – δ^2H were measured in water present in tiny primary fluid inclusions trapped in Mesoproterozoic (≈ 1.4 Ga) and Neoproterozoic (≈ 0.8 Ga) halite crystals. While the hydrogen concentrations range from 300 to 1500 ppm for the whole sample collection, δ^2H values range from -74 ‰ to -54 ‰ (VSMOW) for the Mesoproterozoic halite sampled from the Sibley Group, Ontario, Canada, and from -89 to -38 ‰ for the Neoproterozoic halite from the Browne Formation, Officer Basin, Australia. The amount of evaporation required to precipitate halite is accompanied by a deuterium-enrichment of 30 ‰ to 90 ‰. It means that the original aqueous solutions had δ^2H values comprised between -140 ‰ and -90 ‰. Considering the estimated tropical paleolatitudes for both depositional environments, surface waters were most likely significantly deuterium-depleted relative to modern ones. If such interpretation is partly at variance with the geological record, it could be reconciliated with some modelling outputs of the long-term water cycle. Indeed, several mechanisms produce a progressive deuterium-enrichment of the oceans. Those identified so far are the addition of deuterium-rich extraterrestrial water (cometary dust), the loss of H during water photodissociation by ultraviolet radiation in the upper atmosphere, and the isotopic fractionation that takes place during the hydroxylation of nominally-anhydrous mantle rock-forming minerals. We also propose that the major process able to shift through time the δ^2H of the hydrosphere is the reduction of H_2O into H_2 during the serpentinization of mantle rocks at mid-ocean ridges.

1. Introduction

Knowledge of the global water cycle is of paramount importance regarding the dynamics of mass transfer between the Earth's layers and the distribution of water among the main reservoirs. Indeed, the two main water reservoirs are the mantle and the oceans, while smaller but non-negligible amounts of freshwater are linked to the presence of continental masses (ice caps, glaciers, groundwaters, lakes). For decades, stable isotope compositions (δ^2H and $\delta^{18}O$) of the water molecule have been recognized as useful tracers of the Earth's surface water cycle (Craig, 1961; Craig and Gordon, 1965) in relation to the heat balance that triggers climate change. Global scale processes related to Earth's internal dynamics have the potential to affect the isotopic composition of seawater. For instance, changes in seafloor spreading and subduction rates modify the rate of water transfer between the mantle and oceanic reservoirs. Changes in the depth of hydrothermal interaction between seawater and the oceanic lithosphere modify the amount of water that can be cycled into the mantle. The growth of geochemical reservoirs, like the continental crust or the ice caps, may also change the mass and isotopic compositions of the oceans.

The knowledge of the stable isotope composition of the past hydrosphere represents a major issue as it reflects changes in the dynamics of the global water cycle. Therefore, the oxygen isotope composition of past oceans has been investigated through the study of ophiolites (Gregory and Taylor, 1981; Holmden and Muehlenbachs, 1993) and marine sediments (Veizer et al., 1997; Kasting et al., 2006), and was also the object of numerical modelling (e.g., Lécuyer and Allemand, 1999; Wallmann, 2001; Hren et al., 2009; Pope et al., 2012). The debate has been vigorous between the proponents of ^{18}O-depleted (relative to SMOW) and "cold" Precambrian oceans and those supporting the theory of modern-like seawater $\delta^{18}O$ and "warm" oceans. However, Came et al. (2007) argued for a constant $\delta^{18}O$ of oceans throughout the Phanerozoic and, recently, Tartèse et al. (2017, page 55) reported

oxygen isotope compositions of carbonaceous matter indigenous to Precambrian cherts and showed that "the oxygen isotope composition of seawater during most of the Precambrian remained around 0±5‰ consistent with the composition of present-day seawater". The main process that maintained the steady-state $\delta^{18}O$ value of the oceans is the buffering through isotopic exchange between seawater and oceanic crust during hydrothermal alteration (Muehlenbachs and Clayton, 1976; Gregory and Taylor, 1981).

By contrast, the $\delta^{2}H$ of the oceans was likely not steady over time, especially during the Precambrian, as supported by some geological data (Pope, 2011 and references therein) and flux modelling outputs (Lécuyer et al., 1998; Genda and Ikoma, 2008; Kurokawa et al., 2018). However, $\delta^{2}H$ values of hydrothermally-altered past oceanic rocks (ophiolites, greenstone belts) are tricky to interpret as they result from a combination of several variables such as the temperature of isotopic exchange, the amount of water reacting with rock, and the initial $\delta^{2}H$ of reacting rock and water. Not least is the issue of the preservation of the hydrogen isotope compositions of these old rocks. In most cases, hydrogen isotope measurements were performed on serpentine minerals for which Kyser and Kerrich (1991) showed that hydrous minerals are prone to retrograde isotopic exchange with water at low temperature. This property may partly explain why serpentines of any geological age display large ranges ($\geq$ 50‰ in most cases) of $\delta^{2}H$ values without showing any kind of secular trend (see Figure 4.1 in Pope, 2011).

In the case of modelling, the magnitude and rates of isotopic changes are still poorly constrained because of the large uncertainties associated with all the input and output fluxes connecting the oceanic reservoir (Lécuyer et al., 1998; Genda and Ikoma, 2008; Kurokawa et al., 2018). However, there is an emerging consensus toward the paradigm of a deuterium-depleted Precambrian oceanic reservoir. Indeed, to a first approximation, we can consider that the two main fluxes of water are regulated by plate tectonics. Seawater is incorporated in the

oceanic crust during hydrothermal alteration while it is partly released during dehydration of subducted plates and hotspot volcanism (Kasting and Holm, 1992). Hydrogen isotopes fractionate between free water and hydroxyl groups of minerals at all metamorphic temperatures (Suzuoki and Epstein, 1976). The light isotope is preferentially incorporated into the solid phase leaving the residual water enriched in deuterium. Mass balance and kinetic treatments of the long-term water cycle suggested that the δ^2H value of Archean oceans could have been a few tens of permil lower than the present-day value (Lécuyer et al., 1998; Kurokawa et al., 2018). This result could be explained by the imbalance between fluxes of water trapped at ridges and released along subduction zones (Korenaga et al., 2017), by the reduced size of continental masses (Condie and Kröner, 2013), and the absence of ice sheets (Ramstein, 2011). Moreover, a progressive deuterium-enrichment of the oceans has been proposed through an addition of water via impacts of extra-terrestrial bodies and the escape of atomic H to space by photodissociation of the water in the upper atmosphere (Lécuyer et al., 1998; Genda and Ikoma, 2008).

As both modelling approach and isotopic measurement of hydrous minerals cannot provide reliable magnitudes of δ^2H change through time, a more appropriate way to decipher the hydrogen isotope composition of past surface waters is to analyze their fossil remnants trapped in minerals during their growth. Indeed, surface waters are commonly trapped as tiny fluid inclusions in the crystal lattice defects of various neoformed minerals. Fluid inclusions, indeed, represent a unique opportunity for a straightforward determination of some past climatic parameters (air and water temperatures, air humidity) and the chemical and isotopic compositions of both ocean and atmosphere. Fluid inclusions were used, for example, to estimate paleoaltitudes during the evolution of mountain belts (Blisniuk and Stern, 2005; Mulch and Chamberlain, 2007; Johnston et al., 2018) by analyzing quartz-fill in fractures of crustal rocks. Fluid inclusions in calcite precipitated as speleothems in caves were also

studied to reconstruct past mean air temperatures (Schwarcz et al. 1976; Harmon et al., 1979; Matthews et al. 2000; Dennis et al. 2001; McGarry et al., 2004; Verheyden et al., 2008; Griffiths et al., 2010; Arienzo et al., 2013; Blamey et al., 2016a; Affolter et al., 2019). Seawater inclusions in marine carbonates provide an opportunity to analyse chemical variations of both ancient atmosphere and ocean (Johnson and Goldstein, 1993). Residual evaporated waters are also trapped in evaporitic minerals and especially within one of critical interest, NaCl (halite), which is nominally H– and O–free. Therefore, fluid inclusions in sedimentary halite from marine evaporite formations were used to estimate changes in chemical composition of Proterozoic (Kovalevych et al., 2006) and Phanerozoic seawater (Kovalevych et al., 1998, Lowenstein et al., 2001, Horita et al., 2002, Brennan and Lowenstein, 2002, Petrychenko et al., 2005; Timofeeff et al., 2006; Brennan et al., 2013; Meng et al., 2018). More recently, they have been used to quantify the Neoproterozoic molecular oxygen partial pressure of the Earth's atmosphere (Blamey et al., 2016b). Hydrogen and oxygen isotope compositions of water inclusions in halite were also determined in order to identify fluid sources and mixing processes (Knauth and Beeunas, 1986; Horita 1990; Yang et al. 1995; Rigaudier et al., 2011).

In this study, we measured the deuterium content in water present in tiny primary fluid inclusions trapped in Mesoproterozoic (≈ 1.4 Ga) and Neoproterozoic (≈ 0.8 Ga) halite crystals in order to decipher whether or not the Proterozoic hydrosphere was deuterium-depleted relative to present-day's.

2. Material and methods

2.1. Sample collection and geological setting

2.1.1. Neoproterozoic Browne Formation, Australia

We studied halite samples from the Lancer 1 and Empress 1A drill cores located close to each other in the northwestern part of the Officer Basin (Figure 1). Halite was sampled in the "B" interval of the Browne Formation whose age is constrained between 800 and 830 Ma on the basis of $\delta^{13}C$ and $^{87}Sr/^{86}Sr$ global correlations, and U/Pb zircon dating of the Gairdner Dyke Swarm (827±6 Ma; Wingate et al., 1998) and the Rook Tuff (802±10 Ma; Fanning et al., 1986). Stevens and Apak (1999) described the sedimentary succession at Empress-1A, it is made of evaporites such as gypsum, anhydrite and halite along with calcareous shales, sandstones, dolomitic limestones and stromatolitic dolomites. Townson (1985) and Carlsen et al. (1999) proposed that this sedimentary sequence was deposited in a shallow marine environment, possibly an interior sea, with prevailing hot and dry climatic conditions. Those marine waters were, however, regularly subject to freshwater excursions to generate brief episodes of brackish water. Townson (1985) also proposed that these sedimentary series reflect the ephemeral existence of coastal lakes, e.g., like playa lakes that occur in the present-day Southern High Plains of the United States or in the Ebro Basin (Salvany et al., 1994).

2.1.2. The Mesoproterozoic Sibley Group, Canada

Halite samples were obtained through drilling of the Mesoproterozoic sedimentary rocks of the Sibley Group that crops out between Lake Nipigon and Lake Superior, northern Ontario, Canada (Figure 2). According to Rogala et al. (2007), U-Pb zircon dating indicates a maximum age of depostion of 1443±31 Ma and the sedimentary succession resembles that documented in the Neoproterozoic Browne Formation, Australia. Indeed, the deposits consist of alternating silstones and dolostones, which indicate hydrological cyclic variations of the lacustrine system (Talbot and Allen, 1996). Nodular chert, calcite blebs and the increasing occurrence of evaporites reflect the transition from a lacustrine or deltaic environment to an

ephemeral playa lake during intense periods of aridity (Cheadle, 1986; Rogala et al., 2007). The uppermost lacustrine strata that represent the area that the salt would come from record an abrupt increase of $\delta^{34}S$ from from 5 ‰ to 12 ‰ (CDT) and the Y/Ho ratio increases as well (Metsaranta, 2006). Both of these geochemical data indicate the possibility of a limited marine incursion in the upper Channel Island member of the Rossport Formation, which represents the time interval that the lake shrank and dried up, ie. when the salt was deposited.

2.2. Integrity of halite fluid inclusions

Only halite samples from the Neoproterozoic Browne Formation and from the Mesoproterozoic Sibley Group, which fullfilled the multi-step screening method developed by Blamey and Brand (2019) for selecting the most pristine halite crystals, were selected for the determination of water $\delta^{2}H$. Detailed methods and results are given in Blamey et al. (2016b), Blamey and Brand (2019) and Blamey et al. (2018). In summary, the halite samples satisfied the following criteria with the associated outputs:

1) Petrography for studying that support the preservation of primary fluid inclusions, Petrography was used to identify and select sub-samples that only contain primary fluid inclusions based on fabrics and texture such as chevron bands, cornets, and hoppers (see photomicrographs published in Blamey and Brand, 2019). Most fluid inclusions have sizes ranging from 5 μm to 50 μm (see photomicrographs published in Blamey et al., 2016b and Blamey et al., 2018).
2) Microthermometry to define the range of temperature of crystallization. Homogenization temperatures obtained for the Tonian Browne Formation are comprised between 40°C and 47°C (Blamey and Brand, 2019), while those for the Ectasian-Calymmian Sibley Group range from 22.3°C to 33.7 ˚C (Blamey et al.,

2018). Such temperatures are compatible with low latitude Earth's surfaces exposed directly or not to the Sun.

3) Trace element (Br, Ca, Mg, Sr), and sulfur and strontium isotope geochemistry to check the preservation of seawater chemistry in the case of evaporites of marine origin. Both studied salt deposits suggest the presence of a marine component, more particularly for the Browne Formation (Blamey et al., 2016b).

4) Argon isotope geochemistry to track any possible leakage of gas from fluid inclusions. Elevated $^{40}Ar/^{36}Ar$ values relative to modern atmosphere for the ancient samples reflect in situ production of radiogenic argon by the decay of ^{40}K housed in fluid inclusions. Data suggest that fluid inclusions behaved as closed systems with respect to argon since their deposit about 1.4 Ga and 0.8 Ga ago, respectively (Blamey et al., 2016b; Blamey and Brand, 2019; Blamey et al., 2018).

2.3. Isotopic analysis of halite fluid inclusions

2.3.1. Limit of the method

Off-line techniques (Kishima and Sakai, 1980; Vennemann et al., 1993; Lécuyer et al., 1994; Morrison et al., 2001) allow to determine both δ^2H and $\delta^{18}O$ ratios (‰ VSMOW) of water inclusions pending that large amounts (several grams) of halite crystals are available per aliquot. Unfortunately, such amount is not available for samples obtained from drilling cores, particularly after a cautious selection of the grains that preserved primary fluid inclusions. Only a few tens of milligrams can be used for the isotopic analysis. Theoretically, both isotopic measurements could be performed on-line using carbon-based reactors that potentially provide oxygen as CO and hydrogen as H_2 for isotopic analysis. However, Gehre et al. (2017), have shown that an accurate hydrogen isotopic analysis of halogen-bearing matrices is precluded because of the "*formation of hydrogen-bearing reaction products other*

than molecular hydrogen (H_2) responsible for non-quantitative H_2 yields and possible hydrogen isotopic fractionation". So far, only Cr-based reactors are able to provide an accurate $^2H/^1H$ determination of water inclusions in halite (Fourel et al., 2019). However, the measurement of the oxygen isotope ratio is compromised because H_2 is obtained by reduction of H_2O in presence of Cr metal at high temperature within the reactor of the elemental analyzer, which means that oxygen reacts with Cr to form Cr_2O_3.

2.3.2. Instrumental configuration for the δ^2H measurement of water inclusions

The protocol used in this study was directly inspired by the one originally proposed by Fourel et al. (2019). In summary, δ^2H measurements of water trapped as inclusions in halite were performed using a Pyrocube® Elemental Analyser (Elementar GmbH-Germany) connected online in continuous flow mode to an IsoPrime IRMS. We used a method where the Pyrocube® elemental analyzer operating at a pyrolysis temperature of 1450°C was configured with a chromium-based ceramic reactor allowing the δ^2H of halite fluid inclusions to be measured accurately (Fourel et al., 2019). Measurements were calibrated using reference material (Gerstenberger and Herrmann, 1983; Hut, 1987; Coplen et al., 2006) IAEA-CH7 (δ^2H = −100.3±2.0 ‰ VSMOW), NBS22 (δ^2H = −120±1 ‰ VSMOW; Silverman, 1964; Coplen et al., 2006; Qi et al., 2004), NBS30 (δ^2H = −65.7±0.3 ‰ VSMOW; Gonfiantini, 1984), the Pollen working standard (δ^2H = −156.1±2.0 ‰ VSMOW, J. Morrison, personal communication, 2017), L-tryptophane (δ^2H = −48±3 ‰ VSMOW, P. Jame, personal communication, 2017), and L-valine (δ^2H = −101±3 ‰ VSMOW, P. Jame, personal communication, 2017).

Grain size of halite samples is close to 1 mm, large enough to analyze both small and large fluid inclusions. The use of larger grain size may preclude the decrepitation of all fluid inclusions. This method has been already tested with success by analyzing 10 mg aliquots of

241 synthetic halite crystals with known δ^2H from their fluid inclusions having H concentrations
242 at the 0.2% level (Fourel et al., 2019). The reproducibility associated with these
243 measurements was close to ±3 ‰. In the case of the Proterozoic halite samples, aliquot size
244 ranged from 50 to 80 mg of halite because they contain less water than synthetic halite. For
245 each halite sample, repeated measurements (n = 3 or 4) provided standard deviations (S.D.)
246 from 2.5 ‰ to 8.8 ‰ with an average value of 5.5 ‰ (Table 1), which is higher than those
247 obtained for the reference materials (0.3 < S.D. < 3.0).
248
249 3. δ^2H and [H] of Precambrian halite fluid inclusions
250 The eight samples of halite from the Mesoproterozoic Sibley Group have δ^2H values
251 ranging from -74 ‰ to -54 ‰ (VSMOW) with a mean value of -61.9±17.2‰ and H
252 concentrations comprised between 44 and 186 ppm (mean = 150±92). The six samples from
253 the Neoproterozoic Browne Formation have δ^2H values that range from -89 ‰ to -38 ‰ with
254 a mean value of -63.5±7.2‰ and H concentrations comprised between 80 and 324 ppm
255 (mean = 104±51). We observe that there is no significant correlation between the δ^2H and H
256 concentrations for samples from either the Sibley Group (R^2 = 0.11; n = 8) or the Browne
257 Formation ($R^2 = 10^{-4}$; n = 6) (Figure 3).
258
259 4. Discussion
260 4.1.1. Extraction of fluid inclusions from halite: validity of the method
261 Depending on the choice of extraction techniques of fluid inclusions from halite, the
262 recovery of water and the integrity of its stable isotope compositions may be a sensitive issue
263 as demonstrated by Horita and Matsuo (1986). Especially in the case of melting techniques or
264 high-temperature decrepitation (the case in this study), the H and O isotope ratios of released
265 fluids can be compromised owing various reactions that may take place at such high-

266 temerature of 1450°C. There is a safe way, however, to check if the measured δ^2H values
267 reflect those of water inclusions in halite. It consists in analyzing the δ^2H of the water
268 extracted from synthetic halite crystals precipitated in the laboratory and to compare it with
269 the composition of the mother water from which halite crystallized (Horita and Matsuo, 1986;
270 Rigaudier et al., 2011; Fourel et al., 2019). Thus, for example, Rigaudier et al. (2011)
271 observed that the δ^2H of evaporating waters sampled between the stage of halite nucleation
272 and that of final stage of crystallization bracket the compositions of water inclusions in halite.
273 Indeed, as water inclusions are continuously trapped in the defects of the halite crystal lattice
274 throughout their growth, they record the isotopic composition of the residual waters across a
275 time range during which the isotopic values of the water still evolve. This mechanism of
276 crystal growth and fluid inclusion trapping explains the standard deviation exceeding the
277 instrumental error we observe for calibrated materials (see section 2.3.3). For example,
278 crystallization of halite performed outdoor by Fourel et al. (2019) revealed that the mean δ^2H
279 value (+15.8±6.6‰) of halite fluid inclusions lies between the values of evaporating waters at
280 the beginning (+8.3±0.7‰) and end (+19.5±1.4‰) of halite formation.
281
282 4.1.2. Meaning of the large variations in δ^2H
283 The relatively large δ^2H ranges measured either for the Browne Formation or Sibley
284 Group halite samples could either record a progressive leaking of fluid from the halite
285 inclusions or the evolution of an evaporating water mass. The absence of correlation between
286 the δ^2H values and the amount of water trapped in halite constitutes a criterion against leaking
287 fluid inclusions through time. Indeed, fluid inclusion leakage is expected to generate isotopic
288 fractionation during water loss according to a process of Rayleigh distillation. Therefore, we
289 consider further in the discussion that the most likely interpretation of such a range in δ^2H

values of halite fluid inclusions results from the progressive evaporation of a water mass during the nucleation and growth of halite crystals.

4.2. Possible sources of water trapped in Proterozoic halite

Sedimentary environments of the Neoproterozoic Browne Formation and Mesoproterozoic Sibley Group suggest that surface waters may have been mixtures of seawater and freshwater in unknown proportions at time of halite deposition. In the case of the 1.4 Ga halite of the Sibley Group, Canada, a fresh water lake environment has been proposed by Rogala et al. (2007). However, the abrupt increase of $^{34}S/^{32}S$ ratios up to +12 ‰ recorded at the top of the sequence suggests a possible marine input at time the salt was deposited. Indeed, such $\delta^{34}S$ value is comparable to those measured by Strauss (1993) and Strauss and Veizer (2008) for the same geological period.

In the case of the 800 Ma halite of the Browne Formation of the Officer Basin located in Western Australia, a marine environment has been proposed on the basis of sulfur and strontium isotope data (Blamey et al., 2016b; Zaky et al., 2019). Indeed, those halites have $\delta^{34}S$ of +15‰ that are close to the value of +17‰ proposed by Canfield (2005) for Neoproterozoic seawater. However, as seawater is a highly concentrated aqueous solution relative to fresh waters (rainfall, rivers, lakes), it buffers the isotopic ratios of brackish waters even for mixtures largely dominated by the freshwater end-member. Let us consider a mixture of seawater (sw) and river water (rw) with a $[S]_{sw}/[S]_{rw}$ ratio of 340 (similar to present-days; Brown et al., 1989) and $\delta^{34}S$ of +17‰ and 5‰ (Strauss and Veizer, 2008), respectively. Such mixture will have a $\delta^{34}S$ of +15‰ even though its seawater fraction will be only 0.02.

In terms of hydrogen isotope ratios, such mixture will be dominated by the composition of the freshwater end-member because the hydrogen molar ratio between both

315 end-members is one. Consequently, the δ^2H of halite water inclusions will be powerful to
316 detect any presence of freshwater during evaporitic stages of the basin. Such isotopic
317 signatures should strongly depend on the latitudes of these deposits considering the known
318 physical processes that trigger the surface water cycle.

319 Paleomagnetic studies performed by Li and Evans (2011), Wen et al. (2013) and
320 Pisarevsky et al. (2013) allowed these authors to reconstruct paleogeographic maps that locate
321 Australia 800 My ago, and Canada 1.4 Gy ago, within the intertropical belts (Figure 4).
322 Assuming tropical temperatures similar to present-days, those Proterozoic shallow waters
323 submitted to evaporation became most likely deuterium-enriched by about 30 ‰ to 90 ‰
324 (median = +50 ‰) during the course of halite crystallization. Indeed, such range of
325 deuterium-enrichment was measured by (Rigaudier et al., 2011) who measured Messinian
326 halites from Sicily, Italy, and which precipitated at temperatures close to 35°C according to
327 microthermometric data. Accordingly, it means that the initial δ^2H values of those
328 Proterozoic waters were initially comprised between -140 ‰ and -90 ‰ (VSMOW).

329 Even in the case of the extreme scenario that Proterozoic halite was deposited in
330 freshwater-dominated or pure freshwater environments, such values are much lower than
331 those documented today within the intertropical belt with δ^2H values of meteoric waters
332 ranging from -47 ‰ to +8 ‰ along the island coasts and from -45 ‰ to -3 ‰ along the
333 continental coasts according to the IAEA–WMO database (Figure 5). Consequently, on the
334 basis of our current knowledge of the water cycle, such low Proterozoic δ^2H values do not
335 appear compatible with the intertropical paleo-position of both studied Mesoproterozoic and
336 Neoproterozoic sedimentary sequences.

337 One possible interpretation is to consider that the playa lakes were fed by fluvial
338 waters of which the ultimate source would have been located at high altitude. However,
339 today, even Himalayan rivers, which are located between 24°N and 28°N, have $\delta^{18}O$ values

uniformly distributed between -11 ‰ and -6 ‰ (Gajurel et al., 2006), which roughly correspond to δ^2H values between -80 ‰ and -40 ‰ according to the Global Meteoric Water Line (Dansgaard, 1964). These isotopic compositions remain lower than those that fed the Proterozoic playa lakes.

We can also consider that the mother water of evaporites was a highly saline groundwater, which means that less evaporation would be necessary for halite precipitation. If such hypothesis cannot be fully excluded, it remains however unlikely as there is no geological evidence for supporting it.

A challenging interpretation is to postulate that Proterozoic meteoric waters derived from a deuterium-depleted oceanic source. Indeed, such meteoric waters would have derived from an oceanic reservoir depleted by several tens of ‰ relative to SMOW, thus implying geological or extra-terrestrial processes responsible for an increasing deuterium-enrichment of seawater through time.

4.3. Plate tectonics and the isotopic imbalance between mantle and seawater

First of all, plate tectonics removes "water" from the oceans as OH^- during the hydroxylation of mid-ocean ridge basalts. Indeed, significant amounts of water (between 0.4 and 4 times the present mass of the oceans) are stored in the Earth's mantle in both hydrous and anhydrous minerals (Michael, 1988; Finger et al., 1989; Bell and Rossman, 1992; Thompson, 1992; Langmuir, 1994; Hirschmann, 2006). Most of this water is concentrated in the Mantle Transition Zone dominated by minerals such as wadsleyite and ringwoodite that may contain up to 3 wt% of water (Pearson et al., 2014; Fei et al., 2017). The origin of this water could be a mixture between juvenile and surface water recycled from Earth's hydrosphere. Indeed, the main metamorphic minerals formed during basalt-seawater hydrothermal interactions are talc, chlorite, serpentine, prehnite and zeolite in replacement of

clinopyroxene, orthopyroxene, olivine and plagioclase. Hydroxylation of nominally-anhydrous minerals (NAM) is characterized by a $^{2}H/^{1}H$ fractionation between mineral and water that ranges from -100 to -30 ‰ depending on crystal lattice and chemistry (Suzuoki and Epstein, 1976; Graham et al., 1984). Outgassing water of mantle origin is quite negligible as most water released at island arcs is recycled surface water trapped into the sediments and hydrothermally-altered oceanic crust of the subducting slab (Plank et al., 2013). Water at Mid-Ocean Ridges is not degassed as the pressure is too high at a depth of about 2000 m. The main source of deep water released to the surface comes from subaerial and aerial intraplate volcanoes (e.g., Foulger, 2005; Mazza et al., 2019). Consequently, imbalance between the rate of entrapment of water during the hydrothermal alteration of basalts at oceanic ridges and the rate of release of water from the mantle during the dehydration of subducting plates is the most likely scenario to happen.

The geological record provides conflicting interpretations, which is most likely due to an indirect estimation of seawater $\delta^{2}H$ through the measurement of rock-forming hydrous minerals (antigorite, lizardite, chrysotile, chlorite) as well as full or partial isotopic re-equilibration during geological events (burial, contact metamorphism, volcanic activity and orogenesis) that involve waters of magmatic, metamorphic or meteoric origin (Sheppard, 1986). A synthetic overview of available data in the literature helps to figure out this key issue.

For example, Taylor and Magaritz (1975) and Taylor (1977) noted that the hydrogen isotope composition of gneisses and granites from the Archean Swaziland cratons are about 30 ‰ lower than those belonging to Phanerozoic batholiths. In addition, Taylor (1977) proposed that these low $\delta^{2}H$ values could be linked to the hydrogen isotope composition of the altered oceanic crust that may have reacted with an ocean whose $\delta^{2}H$ value was closer to -30 ‰ than 0 ‰. In a similar way, we could consider that the low $\delta^{2}H$ values measured in

390 Archean greenstone belts are also compatible with an Archean hydrosphere that was
391 deuterium-depleted in comparison to modern times. Indeed, Pope (2011) measured δ^2H
392 values of Isua (Greenland) serpentines in the range -99 ‰ to -53 ‰. Lécuyer et al. (1994)
393 reported amphibole values from -88 to -77 ‰ for the 3.5 Ga old altered komatiites from the
394 Barberton Greenstone Belt, South Africa, whereas Kyser et al. (1999) measured δ^2H of
395 serpentines from Abitibi, Canada, with a large range from -147 to -54 ‰. It is worth noting
396 that δ^2H values of whole rock samples from a hydrothermally altered layered flow from the
397 Chukotat Group of the Lower Proterozoic (2.0-1.9 Ga) Cape Smith fold belt (northern
398 Quebec) range from -53 ‰ to -40 ‰ (Lécuyer et al., 1996), only matching the highest δ^2H
399 values documented (-80 to -30 ‰) in the modern oceanic crust (Sakai et al., 1990; Agrinier et
400 al., 1995; Früh-Green et al., 1996; Alt and Shanks, 2006. Moreover, many Phanerozoic
401 ophiolites display δ^2H values of serpentine in a global range of -190 to -60 ‰ (Wenner and
402 Taylor, 1973; Magaritz and Taylor, 1974; Burkhard and O'Neil, 1988; Yui et al., 1990;
403 Liakhovitch et al., 2006). Consequently, it appears that the Precambrian record matches the
404 Phanerozoic one with huge isotopic ranges that preclude either any identification of secular
405 trend or any conclusion regarding the hydrogen isotope composition of Precambrian surface
406 waters.
407
408 4.4. Secular unidirectional water fluxes
409 4.4.1. Photodissociation of water in the upper atmosphere
410 The present-day flux of hydrogen escape in the upper atmosphere is about $3x10^8$ atom
411 $H.cm^{-2}.s^{-1}$ (Yung et al., 1989). This flux is three orders of magnitude lower than water fluxes
412 affecting the mantle-ocean system and thus cannot significantly affect the mass of the
413 hydrosphere. Assuming that hydrogen is entirely lost as ^1H with no loss of ^2H , the change in
414 the δ^2H value of the oceans was only +2 to +3 ‰ when integrated over a period of 4.5 Gyr

(Yung et al., 1989; Lécuyer et al., 1998). However, it is unlikely that this flux was constant over time, especially during the Precambrian when the Earth's atmospheric chemistry strongly differed in terms of CO_2, O_2 and H_2 partial pressures. Indeed, Holland (1984) considered that the input H flux to the early Earth was much higher, however, in a poorly-constrained range of 1.9×10^9 to 1.9×10^{13} $cm^{-2}.s^{-2}$, partly resulting from the volcanic activity releasing reduced gases to the atmosphere. Yung et al. (1989) calculated a flux averaged over the Earth's history of 1.3 to 5.8×10^{10} $cm^{-2}.s^{-2}$ lying within the range estimated by Holland (1984). For that purpose, Yung et al. (1989) considered that the $^2H/^1H$ ratio of a deep-sea tholeiitic glass, which trapped and preserved primordial rare gases such as He and Ne (Craig and Lupton, 1976), had a hydrogen isotope ratio reflecting that of primordial water. Following this hypothesis, the hydrogen isotope composition of primordial oceans should have been deuterium-depleted by about -80 ‰ relative to SMOW, thus corresponding to a water loss of about 36 %, and strongly questioning the paradigm of the continental freeboard constancy (e.g., Eriksson, 1999). A deuterium enrichment of the hydrosphere may also have been triggered by a longer residence time of H_2 in an oxygen-poor Proterozoic atmosphere. However, it mainly concerns the Mesoproterozoic with a pO_2 estimated close to 8% to 10% Present Atmopsheric Level (Blamey et al., 2019) while the oxygenation level of the Neoproterozoic atmosphere was high enough, with a PAL value close to 50–60%, to preclude a large atmospheric residence time of molecular hydrogen (Blamey et al., 2016b; Blamey et al., 2019).

4.4.2. Extra-terrestrial addition of water to the Earth

Lécuyer et al. (1998) calculated that the total water mass added to the terrestrial oceans in 4.5 Gyr should lie between 4 and 22 % according to the relative contribution of comets and water-rich carbonaceous chondrites. Considering a maximum possible δ^2H value for this extraterrestrial water of +990±160 ‰, which matches the P/Halley comet composition (Deloule and Robert, 1995; Eberhardt et al., 1995), the δ^2H values of the global ocean should have been close to -10 ‰ (SMOW) 4.2 Gyr ago.

4.4.3. Continental growth and water storage

The sum of meteoric waters stored in the atmosphere, lakes, rivers, soils, and groundwaters is about 3.5 % of the total Earth's surface water (Oki, 2006). The δ^2H value of meteoric waters from the equatorial-tropical to polar areas range from +30 to -260 ‰ but most of the precipitations fall over equatorial and temperate belts, therefore we can estimate an average δ^2H value of -55 ‰ (Lécuyer, 2013). The contribution of this reservoir to the hydrosphere is thus estimated to be close to 2 ‰ and can be reasonably ignored in the mass balance calculation. Lécuyer et al. (1998) calculated a δ^2H value for a continent-free Earth's ocean of -18(±6) ‰ and a mass of $1.7(\pm0.2)\times10^{21}$ kg, about 20 % larger than the present-day mass (1.38×10^{21} kg) of the oceans. This isotopic difference of about -20‰ corresponds to the amount of water stored in the biosphere, the continents, and ice sheets of the modern Earth.

4.4.4. H_2O reduction into H_2 during serpentinization of mantle rocks

It has been recognized that serpentinization of ultramafic rocks within the continental and oceanic lithosphere constitutes a major process of H_2 release to the atmosphere. Indeed, a redox reaction involves the reduction of water to H_2 gas through the oxidation of ferrous to ferric iron (Apps and van de Kamp, 1993). Such chemical reaction is accompanied by a high-

magnitude isotopic fractionation that takes place between H_2O and H_2 during the oxidation of iron-bearing silicates (Simon et al., 2011). As temperatures of serpentinization do not exceed 400°C (Bach et al., 2004; Lamadrid et al., 2017), we calculate $1000\ln\alpha(H_2O–H_2)$ values that increase from about 200 to 450 for temperatures decreasing from 400°C to 100°C (Figure 6) using the isotopic fractionation equation of Simon et al. (2011).

The global annual molar flux of H_2 released to the atmosphere is the subject of various estimates in the literature as this one must also include the serpentinization of both continental and oceanic ultramafic rocks. Rona et al. (2013) estimated a flux at mid-cean ridges of $1.67x10^{11}$ mol $H_2.yr^{-1}$ whereas Lollar et al. (2014) proposed a global flux in the order 10^{10} to 10^{11} mol $H_2.yr^{-1}$. Several authors proposed a global H_2 flux close to 10^{11} mol $H_2.yr^{-1}$ (Canfield et al., 2006; Emmanuel and Ague, 2007; Sleep and Bird, 2007), but higher estimates close to 10^{12} mol $H_2.yr^{-1}$ were recently proposed by Worman et al. (2016). Andreani et al. (2017) argued on the basis of data and modelling that this flux was not constant through time, but started at 160 Ma with "elevated H_2 rates ($>10^{12}$ to 10^{13} mol.yr^{-1}) compared to Late Mesozoic (<160 Ma) rates ($<10^{11} – 10^{12}$ mol.yr^{-1})". Here, we propose a simple mass balance calculation based on a Rayleigh-type distillation equation for estimating the magnitude of deuterium-enrichment of the global ocean over 4.5 Gyr. Accordingly, for a temperature of serpentinization ranging from 150 to 350°C, a deuterium-enrichment in the order of a few tens of permil ($\leq$ 80 ‰) is thus expected for fluxes comprised between 10^{11} and 10^{12} mol $H_2.yr^{-1}$ (Figure 7).

4.5. Cumulative effects and the δ^2H of Proterozoic seawater

The anomalously low δ^2H values obtained for the water trapped into the studied Proterozoic halites could result from the cumulative effects produced by the physico-chemical processes described above:

- addition of extraterrestrial water seems to be negligible in the total isotopic budget of the global ocean
- continental growth only had a restricted impact on the δ^2H of seawater during the Archean as the major part of continents were already formed during the Proterozoic (e.g., Dhuime et al., 2012)
- the absence of ice sheets contributes about -10‰
- photodissociation of water in the upper atmosphere and plate tectonics contributed no more than -20 ‰ according to model outputs about 1.5 Gy ago (Lécuyer et al., 1998; Kurokawa et al., 2018). However, Yung et al. (1989) proposed a deuterium-enrichment up to 80 ‰ by considering higher H_2 fluxes during the photodissociation of water during the Archean.
- another significant contribution (up to 80‰) could be the reduction of water into H_2 during the serpentinization of mantle peridotites. It would imply a H_2 flux ranging from 10^{11} to 10^{12} $mol.yr^{-1}$ in agreement with some recent published estimates.

5. Conclusions

Well-preserved halite crystals from the Neoproterozoic (800 Ma) Browne Formation, Australia, and Mesoproterozoic (1.4 Ga) Sibley Group, Canada, contain water with low δ^2H values ranging from -89 ‰ to -38 ‰ (VSMOW) that cannot be explained in the light of our knowledge of the modern global water cycle. As water strongly evaporates during the course

of halite crystallization, the initial δ^2H of water are estimated to be between -140 ‰ and -90 ‰ (VSMOW). Such values are unlikely considering the tropical positions occupied by both basins during the Proterozoic, however, they could testify of the existence of deuterium-depleted oceans compared to those during Phanerozoic times. Physico-chemical processes potentially responsible for a progressive deuterium-enrichment over time have been reviewed, including water flux imbalance between mantle outgassing and water carried by subducted plates, addition of extraterrestrial water and photodissociation of water in the upper atmosphere. However, the isotopic fractionation of large magnitude that takes place during H_2O reduction into H_2 is a key chemical reaction that accompanies the serpentinization of ultramafic rocks, which could represent the main process responsible for the progressive deuterium-enrichment of the oceans by a few tens of per mil.

Acknowledgements – This study has been founded by the TelluS-SYSTER CNRS Program 2018 (CL). The authors also thank one anonymous reviewer and W. M. White for their valuable and constructive reviews that helped us to improve the scientific content of this study.

References:

Affolter, S., Häuselmann, A., Fleitmann, D., Edwards, R. L., Cheng, H., Leuenberger, M., 2019. Central Europe temperature constrained by speleothem fluid inclusion water isotopes over the past 14,000 years. Sci. Adv. 5, eaav3809.

Agrinier, P., Hékinian, R., Bideau, D., Javoy, M., 1995. O and H stable isotope compositions of oceanic crust and upper mantle rocks exposed in the Hess Deep near the Galapagos Triple Junction. Earth Planet. Sci. Lett. 136, 183–196.

Alt, J. C., Shanks III, W.C., 2006. Stable isotope compositions of serpentinite seamounts in the Mariana forearc: Serpentinization processes, fluid sources and sulfur metasomatism. Earth Planet. Sci. Lett. 242, 272–285.

Andreani, M., García del Real, P., Daniel, I., Wright, N., Coltice, N., 2017. Evolution of spreading rate and H_2 production by serpentinization at mid-ocean ridges from 200 Ma to Present. AGU Fall Meeting Abstracts.

Apps, J.A., Van de Kamp, P.C., 1993. Energy gases of abiogenic origin in the Earth's crust. US Geol. Surv. Prof. Pap. 1570, 81–132.

Arienzo, M.M., Swart, P.K., Vonhof, H.B., 2013. Measurement of $\delta^{18}O$ and $\delta^{2}H$ values of fluid inclusion water in speleothems using cavity ring-down spectroscopy compared with isotope ratio mass spectrometry. Rapid Comm. Mass Spec. 27, 2616–2624.

Bach, W., Garrido, C.J., Paulick, H., Harvey, J., Rosner, M., 2004. Seawater-peridotite interactions: First insights from ODP Leg 209, MAR 15°N. Geochem. Geophys. Geosys. 5(9). doi:10.1029/2004GC000744

Bell, D.R., Rossman, G.R., 1992. Water in Earth's mantle: The role of nominally anhydrous minerals. Science 255, 1391–1396.

Blamey, N., Boston, P. J., Rosales-Lagarde, L., 2016a. High-resolution signatures of oxygenation and microbiological activity in speleothem fluid inclusions. Intern. J. Speleol. 45, 231–241.

Blamey, N., Brand, U., Lécuyer, C., Parnell, J., Heizler, M., Lepland, A., Nic, B., Betus, S., 2019. Goldschmidt Abstracts, pp. 300.

Blamey, N., Brand, U., Parnell, J., Lécuyer, C., Heizler, M., Davis, A., Shaver, K.S., Fralick, P., 2018. Development of a halite screening protocol for ancient atmosphere. Goldschmidt Abstracts, 300.

559 Blamey, N.J.F., Brand, U., 2019, Atmospheric gas in modern and ancient halite fluid
560 inclusions: a screening protocol: Gond. Res. 69, 163–176, doi: 10.1016/j.gr.2018.12.004.
561 Blamey, N.J.F., Brand, U., Parnell, J., Spear, N., Lécuyer, C., Benison, K., Meng, F., Ni, P.,
562 2016b. Paradigm shift in determining Neoproterozoic atmospheric oxygen. Geology 44,
563 651–654. doi:10.1130/G37937.1.
564 Blisniuk, P.M., Stern, L.A., 2005. Stable isotope paleoaltimetry: A critical review. Am. J. Sci.
565 305, 1033–1074.
566 Brennan, S.T., Lowenstein, T.K., Cendón, D.I., 2013. The major-ion composition of
567 Cenozoic seawater: The past 36 million years from fluid inclusions in marine halite. Am.
568 J. Sci. 313, 713–775.
569 Brennan, S.T., Lowenstein, T.K., 2002. The major–ion composition of Silurian seawater.
570 Geochim. Cosmochim. Acta 66, 2683–2700.
571 Brown J., Colling A., Park D., Phillips J., Rothery D., Wright, J., 1989. Seawater: Its
572 composition, properties and behaviour. The Open University. Oxford, Pergamon Press,
573 165 pp.
574 Burkhard, D.J.M., O'Neil, J.R., 1988. Contrasting serpentinization processes in the eastern
575 Central Alps. Cont. Min. Pet. 99, 498–506.
576 Came, R., Eiler, J., Veizer, J. Azmy, K., Brand, U., Weidman, C.R. 2007. Coupling of surface
577 temperatures and atmospheric CO_2 concentrations during the Palaeozoic era.
578 Nature 449, 198–201. https://doi.org/10.1038/nature06085.
579 Canfield, D.E., 2005. The early history of atmospheric oxygen: homage to Robert M.
580 Garrels. Annu. Rev. Earth Planet. Sci. 33, 1–36.
581 Canfield, D.E., Rosing, M.T., Bjerrum, C., 2006. Early anaerobic metabolisms. Phil. Trans.
582 Royal Soc. B: Biol. Sci. 361, 1819–1836.
583 Carlsen, G.M., Apak, S.N., Ghori, K.A.R., Grey, K., Stevens, M.K., 1999. Petroleum
584 potential of the Neoproterozoic western Officer Basin Western Australia based on a
585 source-rock model from Empress 1A. The APPEA Journal 39, 322–342.
586 Cheadle, B., 1986. Alluvial-playa sedimentation in the lower Keweenawan Sibley Group,
587 Thunder Bay District, Ontario. Can. J. Earth Sci. 23, 527–541.
588 Condie, K.C., Kröner, A., 2013. The building blocks of continental crust: evidence for a
589 major change in the tectonic setting of continental growth at the end of the
590 Archean. Gondwana Res. 23, 394–402.
591 Coplen, T.B., Brand, W.A., Gehre, M., Gröning, M., Meijer, H.A.J., Toman, B., Verkouteren,
592 R.M., 2006. New guidelines for ^{13}C measurements. Anal Chem. 78(7), 2439–2441.

593 Craig, H., 1961. Isotopic variations in meteoric waters. Science 133, 1702–1703.
594 Craig, H., Gordon, L.I., 1965. Deuterium and oxygen-18 variations in the ocean and the
595 marine atmosphere. In Stable Isotopes in Oceanographic Studies and Paleotemperatures
596 (ed. E. Tongiorgi). Lab. Geol. Nucl. pp. 9–130.
597 Craig, H., Lupton, J. E., 1976. Primordial neon, helium, and hydrogen in oceanic
598 basalts. Earth Planet. Sci. Lett. 31, 369–385.
599 Dansgaard, W., 1964. Stable isotopes in precipitation. Tellus 16, 436–468.
600 Deloule, E., Robert, F., 1995. Interstellar water in meteorites? Geochim. Cosmochim. Acta
601 59, 4695–4706.
602 Dennis, P.F., Rowe, P.J., Atkinson, T.C., 2001. The recovery and isotopic measurement of
603 water from fluid inclusions in speleothems. Geochim. Cosmochim. Acta 65, 871–884.
604 Dhuime, B., Hawkesworth, C. J., Cawood, P. A., Storey, C.D., 2012. A change in the
605 geodynamics of continental growth 3 billion years ago. Science 335, 1334–1336.
606 Eberhardt, P., Reber, M., Krankowsky, D., Hodges, R.R., 1995. The D/H and $^{18}O/^{16}O$ ratios
607 in water from comet P/Halley. Astron. Astrophys. 302, 301–318.
608 Emmanuel, S., Ague, J.J., 2007. Implications of present-day abiogenic methane fluxes for the
609 early Archean atmosphere. Geophys. Res. Lett. 34, L15810, doi:10.1029/2007GL030532.
610 Eriksson, P.G., 1999. Sea level changes and the continental freeboard concept: general
611 principles and application to the Precambrian. Precamb. Res. 97, 143–154.
612 Fanning, C.M., Ludwig, K.R., Forbes, B.G., Preiss, W.V., 1986. Single and multiple grain U–
613 Pb zircon analyses for the early Adelaidean Rook Tuff, Willouran Ranges, South
614 Australia. 8th Australian Geological Convention, Adelaide, 1986, Abstracts of the
615 Geological Society of Australia 15, 71–72.
616 Fei, H., Yamazaki, D., Sakurai, M., Miyajima, N., Ohfuji, H., Katsura, T., Yamamoto, T.,
617 2017. A nearly water-saturated mantle transition zone inferred from mineral viscosity. Sci.
618 Adv. 3(6), e1603024.
619 Finger, L.W., Ko, J., Hazen, R.M., Gasparik, T., Hemley, R.J., Prewitt, C.T. and Weidner,
620 D.J., 1989. Crystal chemistry of phase B and an anhydrous analogue: implications for
621 water storage in the upper mantle. Nature 341, 140–142.
622 Foulger, G.R., 2005. Plates, plumes, and paradigms. Geol. Soc. Am. 388.
623 doi.org/10.1130/SPE388.

624 Fourel, F., Lécuyer, C., Seris, M., Blamey, N., Brand, U., Fralick, P., Volders, F., 2019.
625 Improved online hydrogen isotope analysis of halite aqueous inclusions. J. Mass Spec. 54,
626 342–350.
627 Früh-Green, G.L., Plas, A. and Lécuyer, C., 1996. Petrologic and stable isotope constraints on
628 hydrothermal alteration and serpentinization of the EPR shallow mantle at Hess Deep (Site
629 895). In: C. Mével, K.M. Gillis, J.F. Allan and P.S. Meyer (Editors), Proc. ODP, Sci.
630 Results, 147: College Station, TX (Ocean Drilling Program), pp. 255–291.
631 Gajurel, A.P., France-Lanord, C., Huyghe, P., Guilmette, C., Gurung, D., 2006. C and O
632 isotope compositions of modern fresh-water mollusc shells and river waters from the
633 Himalaya and Ganga plain. Chem. Geol. 233, 156–183.
634 Gehre, M., Renpenning, J., Geilmann, H., Qi, H., Coplen, T. B., Kümmel, S., Ivdra, N.,
635 Brand, W.A., Schimmelmann, A., 2017. Optimization of on-line hydrogen stable isotope
636 ratio measurements of halogen-and sulfur-bearing organic compounds using elemental
637 analyzer–chromium/high-temperature conversion isotope ratio mass spectrometry (EA-
638 Cr/HTC-IRMS). Rapid Comm. Mass Spec. 31, 475–484.
639 Genda, H., Ikoma, M., 2008. Origin of the ocean on the Earth: early evolution of water D/H
640 in a hydrogen-rich atmosphere. Icarus 194, 42–52.
641 Gerstenberger, H., Herrmann, M., 1983. Report on the intercomparison for the isotope
642 standards limestone KH 2 and polyethylene foil PEF 1. *ZfI-Mitteilungen*. 66, 67–83.
643 Gonfiantini, R., 1984. Advisory group meeting on stable isotope reference samples for
644 geochemical and hydrochemical investigations, IAEA, Vienna, 19-21 September 1983.
645 Report to the Director General. International Atomic Energy Agency, Vienna, Austria.
646 doi:10.1016/0020-708X(84)90059-0.
647 Graham, C.M., Harmon, R.S., Sheppard, S.M.F., 1984. Experimental hydrogen isotope
648 studies IV. Systematics of hydrogen isotope exchange between amphibole and water.
649 Amer. Mineral. 69, 128–138.
650 Gregory, R.T. and Taylor, H.P.J., 1981. An oxygen isotope profile in a section of Cretaceous
651 Oceanic Crust, Samail ophiolite, Oman: evidence for $\delta^{18}O$ buffering of the oceans by
652 deep (>5Km) seawater-hydrothermal circulation at Mid-Ocean Ridges. J. Geophys. Res.
653 86, 2737–2755.
654 Griffiths, M.L., Drysdale, R.N., Vonhof, H.B., Gagan, M.K., Zhao, J.X., Ayliffe, L.K.,
655 Hantoro, WS, Hellstrom, JC, Cartwright, I, Frisia, S., Suwargadi, B.W., 2010. Younger

Dryas–Holocene temperature and rainfall history of southern Indonesia from $\delta^{18}O$ in speleothem calcite and fluid inclusions. Earth Planet. Sci. Lett. 295, 30–36.

Harmon, R.S., Schwarcz, H. P., O'Neil, J.R., 1979. D/H ratios in speleothem fluid inclusions: a guide to variations in the isotopic composition of meteoric precipitation? Earth Planet. Sci. Lett. 42, 254–266.

Hirschmann, M.M., 2006. Water, melting, and the deep Earth H_2O cycle. Annu. Rev. Earth Planet. Sci. 34, 629–653.

Holland, H.D., 1984. The chemical evolution of the atmosphere and oceans. Princeton University Press.

Holmden, C., Muehlenbachs, K., 1993. The $^{18}O/^{16}O$ ratio of 2-billion-year-old seawater inferred from ancient oceanic crust. Science 259, 1733–1736.

Horita J., Zimmermann, H., Holland, H.D., 2002. The chemical evolution of seawater during the Phanerozoic: Implications from the record of marine evaporates. Geochim. Cosmochim. Acta 66, 3733–3756.

Horita, J., 1990. Stable isotope paleoclimatology of brine inclusions in halite: Modeling and application to Searles Lake, California. Geochim. Cosmochim. Acta 54, 2059–2073.

Horita, J., Matsuo, S., 1986. Extraction and isotopic analysis of fluid inclusions in halites. Geochem. J. 20, 261–272.

Hren, M.T., Tice, M.M., Chamberlain, C.P., 2009. Oxygen and hydrogen isotope evidence for a temperate climate 3.42 billion years ago. Nature 462, 205–208.

Hut, G., 1987. Consultants' group meeting on stable isotope reference samples for geochemical and hydrological investigations. Consultants' group meeting on stable isotope reference samples for geochemical and hydrological investigations, International Atomic Energy Agency (IAEA).

Johnson, W.J., Goldstein, R.H., 1993. Cambrian seawater preserved as inclusions in marine low–magnesium calcite cement. Nature 362, 335–337.

Johnston, V.E., Borsato, A., Frisia, S., Spötl, C., Dublyansky, Y., Töchterle, P., Hellstrom, J.C., Bajo, P., Edwards, R.L., Cheng, H., 2018. Evidence of thermophilisation and elevation-dependent warming during the Last Interglacial in the Italian Alps. Sci. Reports 8, 2680. Doi: 10.1038/s41598-018-21027-3.

Kasting, J.F., Holm, N.G., 1992. What determines the volume of the oceans. Earth Planet. Sci. Lett. 109, 507–515.

688 Kasting, J.F., Howard, M.T., Wallmann, K., Veizer, J., Shields, G., Jaffrés, J., 2006.
689 Paleoclimates, ocean depth, and the oxygen isotopic composition of seawater. Earth
690 Planet. Sci. Lett. 252, 82–93.
691 Kishima, N., Sakai, H., 1980. Oxygen-18 and deuterium determination on a single water
692 sample of a few milligrams. Anal. Chem. 52, 356–358.
693 Knauth, L.P., Beeunas, M.A., 1986. Isotope geochemistry of fluid inclusions in Permian
694 halite with implications for the isotopic history of ocean water and the origin of saline
695 formation waters. Geochim. Cosmochim. Acta 50, 419–433.
696 Korenaga, J., Planavsky, N.J., Evans, D.A., 2017. Global water cycle and the coevolution of
697 the Earth's interior and surface environment. Phil. Trans. Royal Soc. A: Mathematical,
698 Physical and Engineering Sciences, 375, 20150393.
699 Kovalevych, V.M., Peryt, T.M., Petrichenko, O.I., 1998. Secular variation in seawater
700 chemistry during the Phanerozoic as indicated by brine inclusions in halite. J. Geol. 106,
701 695–712.
702 Kovalevych, V.M., Peryt T.M., Zang W., Vovnyuk, S.V. 2006 Composition of brines in
703 halite-hosted fluid inclusions in the Upper Ordovician, Canning Basin, Western Australia:
704 new data on seawater chemistry. Terra Nova 18, 95–103.
705 Kurokawa, H., Foriel, J., Laneuville, M., Houser, C., Usui, T., 2018. Subduction and
706 atmospheric escape of Earth's seawater constrained by hydrogen isotopes. Earth Planet.
707 Sci. Lett. 497, 149–160.
708 Kyser, T.K., Kerrich, R., 1991. Retrograde exchange of hydrogen isotopes between hydrous
709 minerals and water at low temperatures. In: Stable Isotope Geochemistry: A Tribute to
710 Samuel Epstein, Taylor Jr, H.P., O'Neil, J.R, Kaplan I.R. (Editors). The Geochemical
711 Society, Special Publication, 3, 409–422.
712 Kyser, T.K., O'Hanley, D.S., Wicks, F.J., 1999. The origin of fluids associated with
713 serpentinization: evidence from stable isotope compositions. Can. Mineral. 37, 223–237.
714 Lamadrid, H.M., Rimstidt, J.D., Schwarzenbach, E.M., Klein, F., Ulrich, S., Dolocan, A.,
715 Bodnar, R.J., 2017. Effect of water activity on rates of serpentinization of olivine. Nat.
716 Comm. 8, 16107. Doi: 10.1038/ncomms16107.
717 Langmuir, C.H., 1994. Water and the solid Earth. Nature 369, 704–705.
718 Lécuyer, C., Allemand P., 1999. Modelling of the oxygen isotope evolution of seawater:
719 implications for the climate interpretation of the $\delta^{18}O$ of marine sediments. Geochim.
720 Cosmochim. Acta 63, 351–361.

721 Lécuyer, C., Gillet, Ph., Robert, F., 1998. Hydrogen isotope composition of seawater and the
722 global water cycle. Chem. Geol. 145, 249–261.
723 Lécuyer, C., 2013. Water on Earth. John Wiley & Sons, 266 pp.
724 Lécuyer, C. Gruau, G., Anhaeusser, C.R., Fourcade, S., 1994. The origin of fluids and the
725 effects of metamorphism on the primary chemical compositions of Barberton komatiites:
726 new evidence from geochemical (REE) and isotopic (Nd, O, H, $^{39}Ar/^{40}Ar$) data. Geochim.
727 Cosmochim. Acta 58, 969–984.
728 Lécuyer, C., Gruau, G., Früh-Green, G., Picard, C., 1996. Hydrogen isotope composition of
729 Paleo-proterozoic seawater. Geology 24, 291–294.
730 Lécuyer, C., O'Neil, J.R., 1994. Stable isotope compositions of fluid inclusions in biogenic
731 carbonates. Geochimica et Cosmochimica Acta, 58, 353–363.
732 Li, Z.X., Evans, D.A., 2011. Late Neoproterozoic 40 intraplate rotation within Australia
733 allows for a tighter-fitting and longer-lasting Rodinia. Geology 39, 39–42.
734 Liakhovitch, V.V., Quick, J.E., Gregory, R.T., 2006. Hydrogen and oxygen isotope
735 constraints on hydrothermal alteration of the Trinity peridotite, Klamath Mountains,
736 California. International Geo. Rev. 47, 203–214.
737 Lollar, B.S., Onstott, T.C., Lacrampe-Couloume, G., Ballentine, C.J., 2014. The contribution
738 of the Precambrian continental lithosphere to global H_2 production. Nature 516, 379–382.
739 Lowenstein, T.K., Timofeeff, M.N., Brennan, S.T., Hardie, L.A., Demicco, R.V., 2001.
740 Oscillations in Phanerozoic seawater chemistry: Evidence from fluid inclusions in salt
741 deposits. Science 294, 1086–1088.
742 Magaritz, M., Taylor, H.P., Jr., 1974. Oxygen and hydrogen isotope studies of
743 serpentinization in the Troodos ophiolite complex, Cyprus. Earth Planet. Sci. Lett. 23, 8–
744 14.
745 Matthews, A., Ayalon, A., Bar-Matthews, M., 2000. D/H ratios of fluid inclusions of Soreq
746 cave (Israel) speleothems as a guide to the Eastern Mediterranean Meteoric Line
747 relationships in the last 120 ky. Chem. Geol. 166, 183–191.
748 Mazza, S.E., Gazel, E., Bizimis, M., Moucha, R., Béguelin, P., Johnson, E.A., McAleer, R.J.,
749 Sobolev, A.V., 2019. Sampling the volatile-rich transition zone beneath
750 Bermuda. Nature 569, 398–403.
751 McGarry, S., Bar-Matthews, M., Matthews, A., Vaks, A., Schilman, B., Ayalon, A., 2004.
752 Constraints on hydrological and paleotemperature variations in the Eastern Mediterranean
753 region in the last 140 ka given by the δD values of speleothem fluid inclusions. Quat. Sci.
754 Rev. 23, 919–934.

Meng, F., Zhang, Y., Galamay, A.R., Bukowski, K., Ni, P., Xing, E., Ji, L., 2018. Ordovician seawater composition: evidence from fluid inclusions in halite. Geol. Quart. 62, 344–352.

Metsaranta, R.T., 2006. Sedimentology and geochemistry of the Mesoproterozoic Pass lake and Rossport Formations, Sibley Group. Unpub. MSc., Lakehead University, 217p.

Michael, P.J., 1988. The concentration, behavior and storage of H_2O in the suboceanic upper mantle: implications for mantle metasomatism. Geochim. Cosmochim. Acta 52, 555–566.

Morrison, J., Brockwell, T., Merren, T., Phillips, A.M., Fourel, F., 2001. On-line high-precision stable hydrogen isotopic analyses on nanoliter water samples. Anal Chem. 73, 3570−3575.

Muehlenbachs, K., Clayton, R.N., 1976. Oxygen isotope composition of the oceanic crust and its bearing on seawater. J. Geophys. Res. 81, 4365–4369.

Mulch, A., Chamberlain, C.P., 2007. Paleoaltimetry: geochemical and thermodynamic approaches. Rev. Min. Geochim. 66, 89–118.

Oki, T., Kanae, S., 2006. Global hydrological cycles and world water resources. Science 313, 1068–1072.

Pearson, D.G., Brenker, F.E., Nestola, F., McNeill, J., Nasdala, L., Hutchison, M.T., Matveev, S., Mather, K., Silversmit, G., Schmitz, S., Vekemans, B., 2014. Hydrous mantle transition zone indicated by ringwoodite included within diamond. Nature 507, 221–224.

Petrychenko, O.Y., Peryt, T.M., Chechel, E.I., 2005. Early Cambrian seawater chemistry from fluid inclusion in halite from Siberian evaporites. Chemical Geology 219, 149–161.

Pisarevsky, S.A., Elming, S.Å., Pesonen, L.J., and Li, Z.X., 2014. Mesoproterozoic paleogeography: supercontinent and beyond. Precamb. Res. 244, 207–225.

Plank, T., Kelley, K.A., Zimmer, M.M., Hauri, E.H., Wallace, P.J., 2013. Why do mafic arc magmas contain~ 4 wt% water on average? Earth Planet. Sci. Lett. 364, 168–179.

Pope, E.C., 2011. Hydrogen and oxygen isotope fractionation in hydrous minerals as indicators of fluid source in modern and fossil metasomatic environments. Stanford University.

Pope, E.C., Bird, D.K., Rosing, M.T., 2012. Isotope composition and volume of Earth's early oceans. Proc. Nat. Acad. Sci. 109, 4371–4376.

Qi, H., Coplen, T.B., Geilmann, H., Brand, W.A., Bohlke, J.K., 2004. Two new organic reference materials for $\delta^{13}C$ and $\delta^{15}N$ measurements and a new value for the $\delta^{13}C$ of NBS 22 oil. Rapid Comm. Mass Spec. 17, 2483–2487.

787 Ramstein, G., 2011. Climates of the Earth and cryosphere evolution. Surv. Geophys. 32, 329.
788 doi.org/10.1007/s10712-011-9140-4
789 Rigaudier, T., Lécuyer, C., Gardien, V., Martineau, F., 2011. The record of temperature, wind
790 velocity and air humidity in the δD and $\delta^{18}O$ of water inclusions in synthetic and
791 Messinian halites. Geochim. Cosmochim. Acta 75, 4637–4652.
792 Rogala, B., Fralick, P.W., Heaman, L.M., Metsaranta, R., 2007. Lithostratigraphy and
793 chemostratigraphy of the Mesoproterozoic Sibley Group, northwestern Ontario, Canada.
794 Can. J. Earth Sci. 44, 1131–1149.
795 Rona, P.A., Devey, C.W., Dyment, J., Murton, B.J., 2013. Diversity of hydrothermal systems
796 on slow spreading ocean ridges. Geophysical Monograph 188, American Geophysical
797 Union, Washington DC.
798 Sakai, R., Kusakabe, M., Noto, M., Ishii, T., 1990. Origin of waters responsible for
799 serpentinization of the Izu-Ogasawara-Mariana forearc seamounts in view of hydrogen and
800 oxygen isotope ratios. Earth Planet. Sci. Lett. 100, 291–303.
801 Salvany, J.M., Munoz, A., Perez, A., 1994 Nonmarine evaporitic sedimentation and
802 associated diagenetic processes of the southwestern margin of the Ebro Basin (Lower
803 Miocene), Spain. J. Sed. Res. 64, 190–203.
804 Schwarcz, H.P., Harmon, R.S., Thompson, P., Ford, D.C., 1976. Stable isotope studies of
805 fluid inclusions in speleothems and their paleoclimatic significance. Geochim.
806 Cosmochim. Acta 40, 657–665.
807 Sheppard, S.M.F., 1986. Characterization and isotopic variations in natural waters. In: J.W.
808 Valley, H.P. Taylor and J.R. O'Neil (Editors), Stable isotopes in high temperature
809 geological processes. Min. Soc. Am., Rev. Min., Vol. 16, pp. 165–183.
810 Silverman, S.R., 1964. In: Craig H., Miller S.L., Wasserburg G.J., eds. Investigations of
811 Petroleum Origin and Evolution Mechanisms by Carbon Isotope Studies. North Holland:
812 Isotopic and Cosmic Chemistry, 92–102.
813 Simon, L., Lécuyer, C., Martineau, F., Robert, F., 2011. Experimental study of D/H
814 fractionation between water and hydrogen gas during the oxidation of Fe-bearing silicates
815 at high temperatures (600°C–1200°C). Centr. Europ. Geol. 54, 81–93.
816 Sleep, N.H., Bird, D.K., 2007. Niches of the pre-photosynthetic biosphere and geologic
817 preservation of Earth's earliest ecology. Geobiol. 5, 101–117.
818 Stevens, M.K., Apak, S.N., 1999. GSWA Empress 1 and 1A Well Completion Report,
819 Yowalga Sub-basin, Officer Basin, Western Australia. Western Australia Geological

820 Survey Record 1999/4. Western Australia Geological Survey, Western Australia. pp. 1–
821 110.
822 Strauss, H., 1993. The sulfur isotopic record of Precambrian sulfates: new data and a critical
823 evaluation of the existing record. Precamb. Res. 63, 225–246.
824 Strauss, H., Veizer J., 2008. Sulfur isotopes. In: Encyclopedia of paleoclimatology and
825 ancient environments. Springer Science & Business Media, pp. 926–929.
826 Suzuoki, T., Epstein, S., 1976. Hydrogen isotope fractionation between OH-bearing minerals
827 and water. Geochim. Cosmochim. Acta 40, 1229–1240.
828 Talbot, M.R., Allen, P.A., 1996. Lakes. In: Sedimentary environments: processes, facies, and
829 stratigraphy. 3rd edition. Edited by H.G. Reading. Blackwell Science, London, UK, 3, 83–
830 124.
831 Tartèse, R., Chaussidon, M., Gurenko, A., Delarue, F., Robert, F., 2017. Warm Archean
832 oceans reconstructed from oxygen isotope composition of early-life remnants. Geochem.
833 Perspec. Lett. 3, 55–65.
834 Taylor, H.P., Jr., Magaritz, M., 1975. Oxygen and hydrogen isotope studies of 2.6 - 3.4 b.y.
835 old granites from the Barberton Mountain Land, Swaziland, and the Rhodesian craton,
836 Southern Africa. Geol. Soc. Am. Abs. Prog. 7, 1293.
837 Taylor, H.P., Jr., 1977. Water/rock interaction and the origin of H_2O in granitic batholiths. J.
838 Geol. Soc. London 133, 509–558.
839 Thompson, A.B., 1992. Water in the Earth's upper mante. Nature 358, 295–302.
840 Timofeeff, M.N., Lowenstein, T.K., da Silva, M.A.M., Harris, N.B., 2006. Secular variation
841 in the major-ion chemistry of seawater: Evidence from fluid inclusions in Cretaceous
842 halites. Geochim. Cosmochim. Acta 70, 1977–1994.
843 Townson, W.G., 1985. The subsurface geology of the western Officer Basin — results of
844 Shell's 1980–1984 petroleum exploration campaign. The Australian Petroleum
845 Exploration Association Journal 25, 34–51.
846 Veizer, J., Bruckschen, P., Pawellek, F., Diener, A., Podlaha, O. G., Carden, G. A., Jasper, T.,
847 Korte, C., Strauss, H., Azmy, K., Ala, D., 1997. Oxygen isotope evolution of Phanerozoic
848 seawater. Palaeogeog. Palaeoclimatol. Palaeoecol. 132, 159–172.
849 Verheyden, S., Genty, D., Cattani, O., van Breukelen, M.R., 2008. Water release patterns of
850 heated speleothem calcite and hydrogen isotope composition of fluid inclusions. Chem.
851 Geol. 247, 266–281.
852 Wallmann, K., 2001. The geological water cycle and the evolution of marine $\delta^{18}O$ values,

Geochim. Cosmochim. Acta 65, 2469–2485.

Wen, B., Li, Y.X., Zhu, W., 2013. Paleomagnetism of the Neoproterozoic diamictites of the Qiaoenbrak formation in the Aksu area, NW China: Constraints on the paleogeographic position of the Tarim Block. Precamb. Res. 226, 75–90.

Wenner, D.B., Taylor, H.P., Jr., 1973. Oxygen and hydrogen isotope studies of the serpentinization of ultramafic rocks in oceanic environments and continental complexes. Amer. J. Sci. 273, 207–239.

Wingate, M.T.D., Campbell, I.H., Compston, W., Gibson, G.M., 1998. Ion microprobe U–Pb ages for Neoproterozoic basaltic magmatism in south-central Australia and implications for the breakup of Rodinia. Precamb. Res. 87, 135–159.

Worman, S.L., Pratson, L.F., Karson, J.A., Klein, E.M., 2016. Global rate and distribution of H_2 gas produced by serpentinization within oceanic lithosphere. Geophys. Res. Lett. 43, 6435–6443.

Yang, W., Spencer, R.J., Krouse, H.R., Lowenstein, T.K., Casas, E., 1995. Stable isotopes of lake and fluid inclusion brines, Dabusun Lake, Qaidam Basin, Western China: Hydrology and paleoclimatology in arid environments. Palaeogeogr. Palaeoclimatol. Palaeoecol. 117, 279–290.

Yui, T., Yeh, H., Lee, C.W., 1990. A stable isotope study of serpentinization in the Fengtien ophiolite, Taiwan. Geochim. Cosmochim. Acta 54, 1417–1426.

Yung, Y.L., Wen, J.S., Moses, J.I., Landry, B.M., Allen, M., Hsu, K.J., 1989. Hydrogen and deuterium loss from the terrestrial atmosphere: A quantitative assessment of nonthermal escape fluxes. J. Geophys. Res. Atm. 94, 14971–14989.

Zaky, A., Brand, U., Buhl, D., Blamey, N., Bitner, A.M., Logan, A., Gaspard, D., Popov, A., 2019. Strontium isotope geochemistry of modern and ancient archives: tracer of secular change in ocean chemistry. Can. J. Earth Sci. 56, 245–264.

878

879 Table captions:

880

881 Table 1: δ^2H (‰ VSMOW) and [H] concentrations of fluid inclusions trapped in the studied

882 Proterozoic halite crystals. Samples L (Lancer1) and E (Empress1A) come from the Officer

883 Basin (Figure 1), Australia (800 Ma), and samples P1 to P8 come from the Mesoproterozoic

884 Sibley Group (Figure 2) (1.4 Ga). S.D. = standard deviation. N = number of measurements.

885

886 Figure captions:

887

888 Figure 1: A) Geographic map of Australia with the location of Officer Basin and the two

889 Lancer 1 and Empress 1A drill cores. B) Sampling horizons in the Browne Formation.

890 Numbers indicate the position of halites that have been measured for the δ^2H (‰ VSMOW)

891 of their water inclusions (Table 1).

892

893 Figure 2: Geographic map of Canada (A) with the location of Thunder Bay (black and red

894 dot), Lake Superior (B), and the outcrop of Sibley Group (C). Samples P1 to P8 belonging to

895 the Outan Island Formation (D), Sibley Group, have been measured for the δ^2H (‰

896 VSMOW) of their water inclusions (Table 1).

897

898 Figure 3: Variations of δ^2H of water inclusions in Proterozoic halites as a function as a

899 function of the amount of hydrogen extracted from the sample by pyrolysis.

900

Figure 4: Various scenarios of Earth paleogeographic reconstructions for the A) Calymnian-Ectasian transition (1.4 Ga) and the B) Tonian (≈ 750 Ma) according to Li and Evans (2011), Wen et al. (2013) and Pisarevsky et al. (2013). Note that for any reconstruction Laurentia and Australia continents are located within the intertropical belt.

Figure 5: Frequency histogram of present-day δ^2H of meteoric waters from tropical islands and continental coasts. Data were extracted from the IAEA–WMO database.

Figure 6: $^2H/^1H$ fractionation between water and dihydrogen during the oxidation of hydrous iron-bearing silicates. The curve was computed according to the experimental study performed by Simon et al. (2011) who determined the following equation: $\alpha(H_2O\text{-}H_2) = 0.2447729(\pm0.027705).10^6.T^{-2} + 1.024(\pm0.022)$.

Figure 7: Deuterium-enrichment of the oceanic reservoir as a function of the H_2 flux released during the serpentinization of continental and oceanic ultramafic rocks. During serpentinization, the oxidation of ferrous iron into ferric iron is accompanied by the reduction of water into dihydrogen. Curves have been computed for three temperatures (T = 150°C with $1000\ln\alpha(H_2O\text{-}H_2) = 2.4085$; T = 250°C with $1000\ln\alpha(H_2O\text{-}H_2) = 1.9297$; T = 350°C with $1000\ln\alpha(H_2O\text{-}H_2) = 1.6623$; see Figure 6) using a Rayleigh distillation equation: $R = R_0 f^{(\alpha-1)}$ with R_o = isotopic ratio of the initial oceanic mass ($1.38x10^{21}$ kg), R = isotopic ratio of the decreasing oceanic mass, f = fraction of the residual oceanic oceanic mass, and α = isotopic fractionation between H_2O and H_2. Fluxes ranging from 10^{11} to 10^{12} H_2 mol.y^{-1} have been

integrated over 4.5 Gyr and correspond to a loss of the oceanic mass ranging from 0.6% to 5.5%.

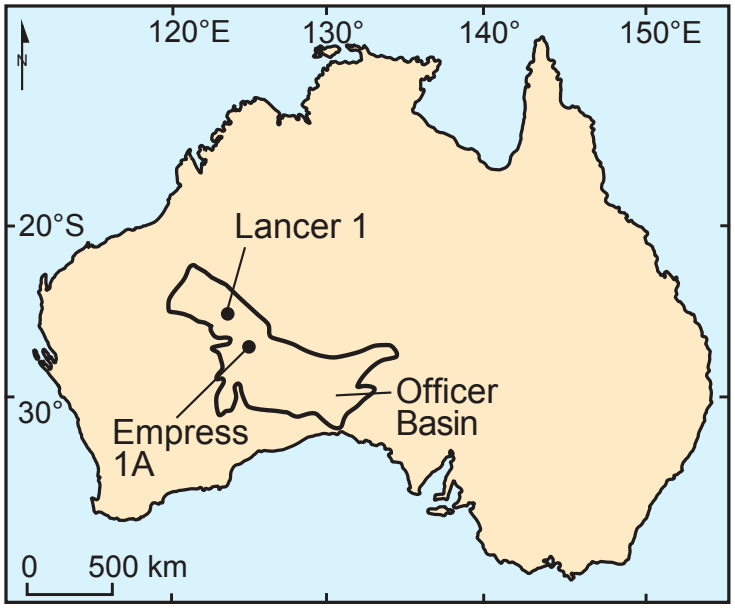
120°E
130°
140°
150°E
20°S
30°
Lancer 1
Empress
1A
Officer
Basin
0
500 km

A)

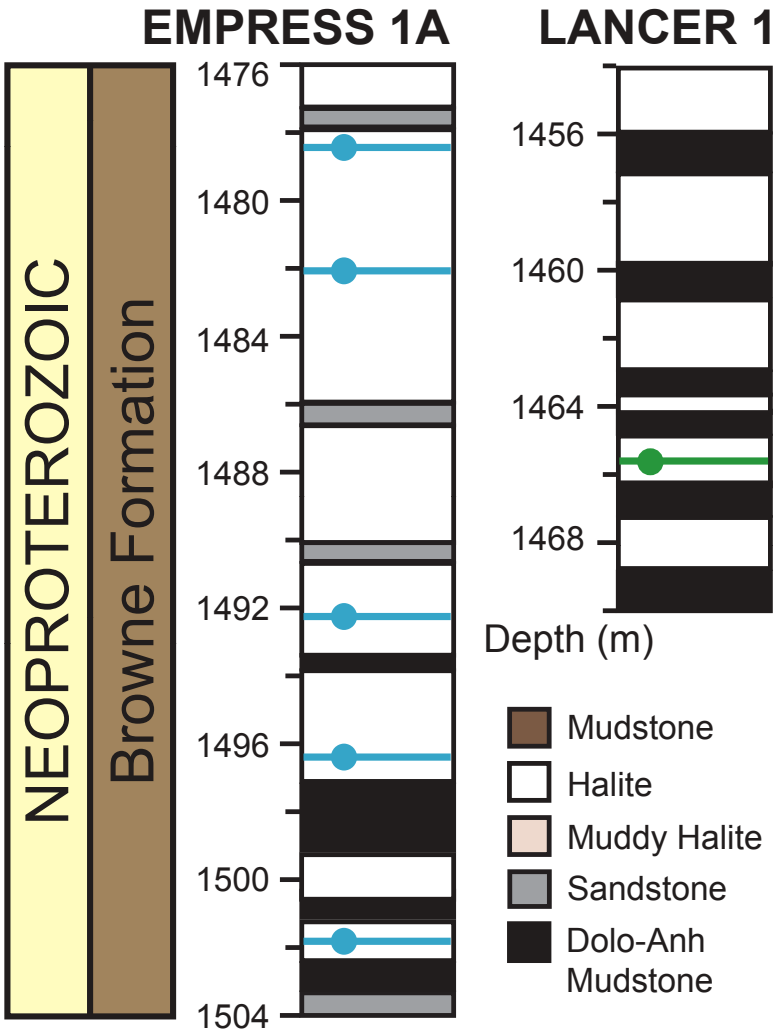
EMPRESS 1A
LANCER 1
NEOPROTEROZOIC
Browne Formation
1476
1480
1484
1488
1492
1496
1500
1504
1456
1460
1464
1468
Depth (m)
Mudstone
Halite
Muddy Halite
Sandstone
Dolo-Anh
Mudstone

B)

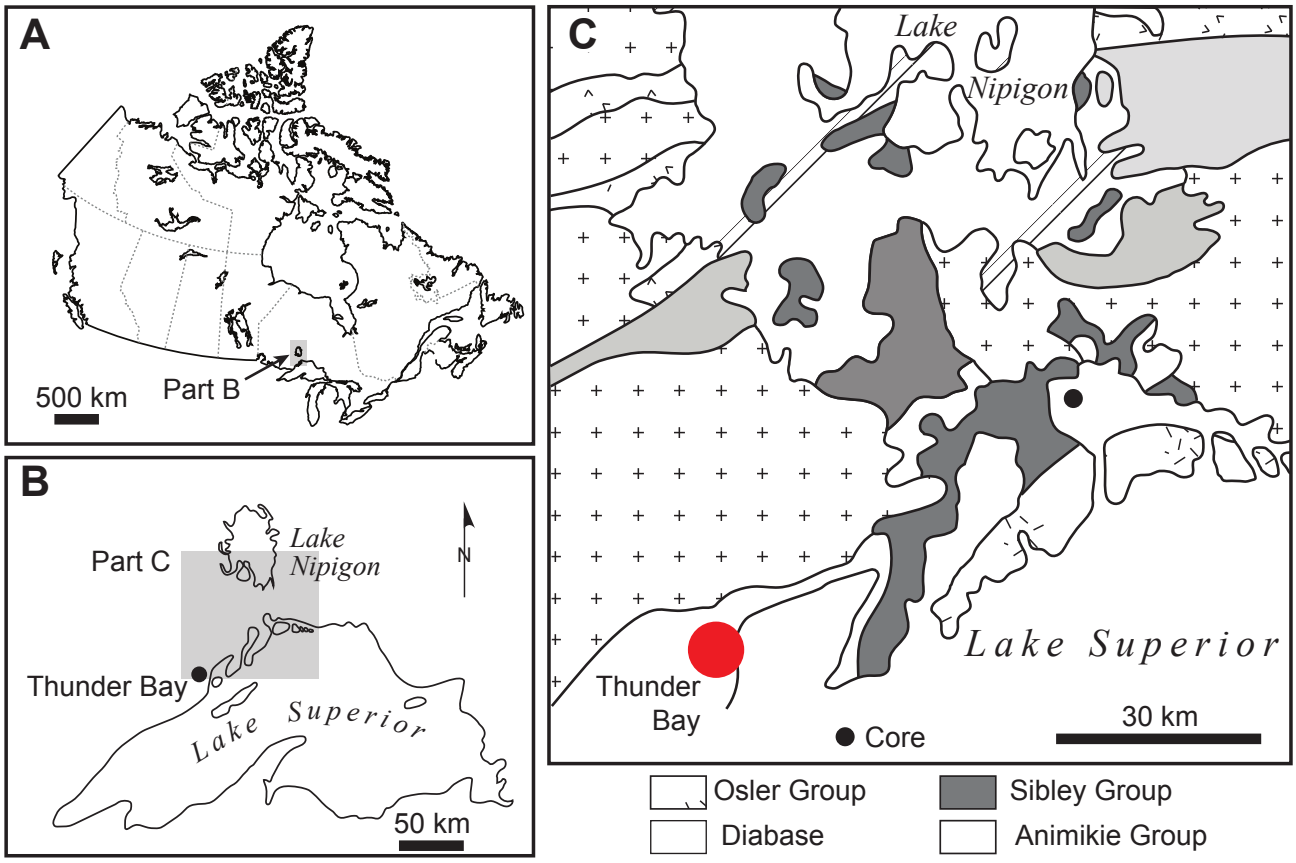
A
500 km
Part B
B
Part C
Lake
Nipigon
N
Thunder Bay
Lake Superior
50 km
C
Lake
Nipigon
Lake Superior
Thunder
Bay
Core
30 km
Osler Group
Sibley Group
Diabase
Animikie Group

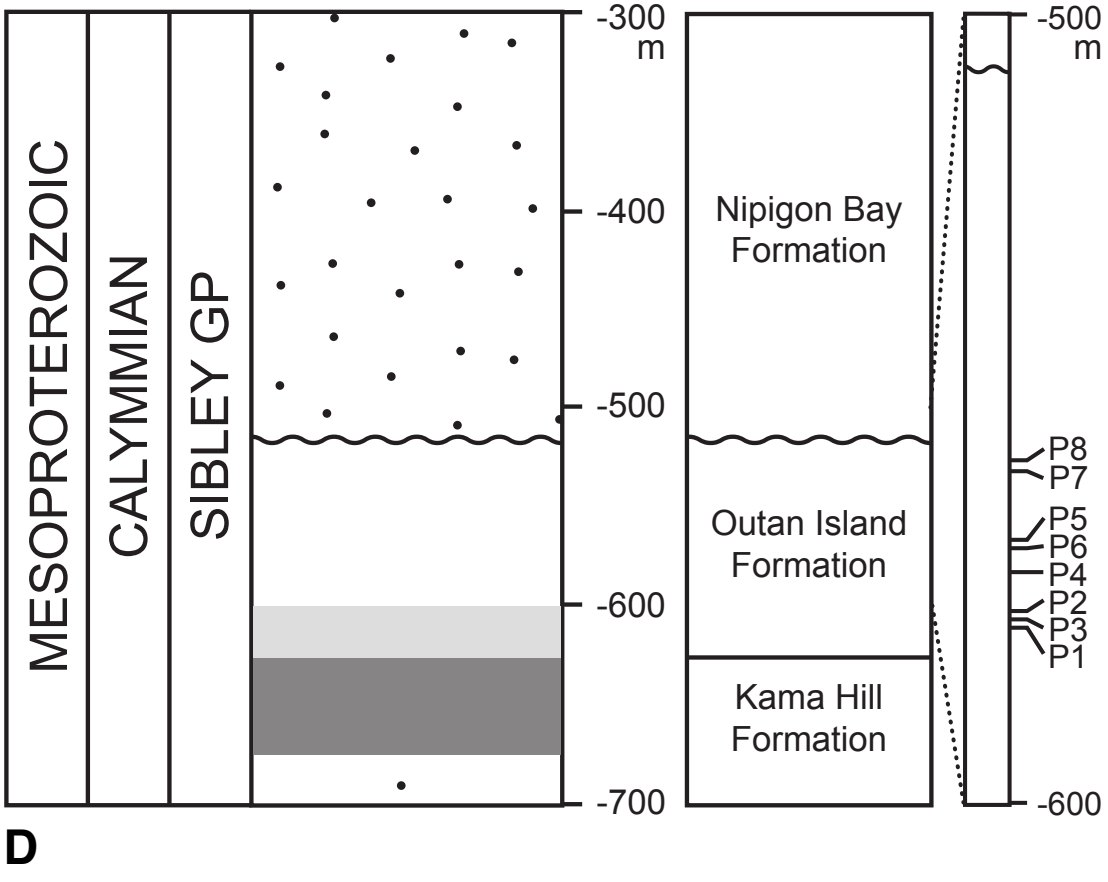
MESOPROTEROZOIC
CALYMMIAN
SIBLEY GP
-300
m
-400
-500
-600
-700
Nipigon Bay
Formation
Outan Island
Formation
Kama Hill
Formation
-500
m
-600
P8
P7
P5
P6
P4
P2
P3
P1

D

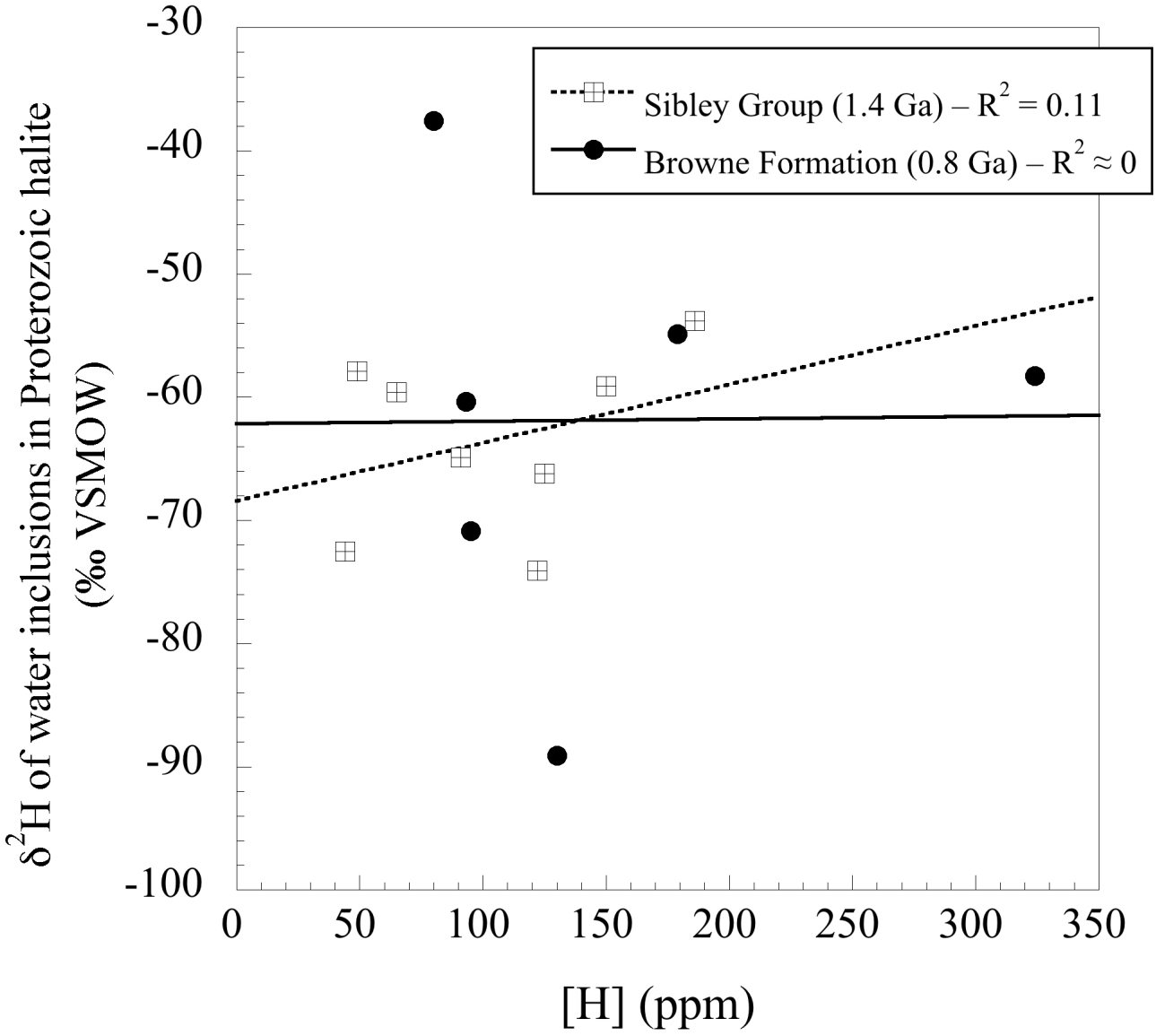
-30
-40
-50
-60
-70
-80
-90
-100
0
50
100
150
200
250
300
350
δ2H of water inclusions in Proterozoic halite (‰ VSMOW)
[H] (ppm)
Sibley Group (1.4 Ga) – R2 = 0.11
Browne Formation (0.8 Ga) – R2 ≈ 0

A)

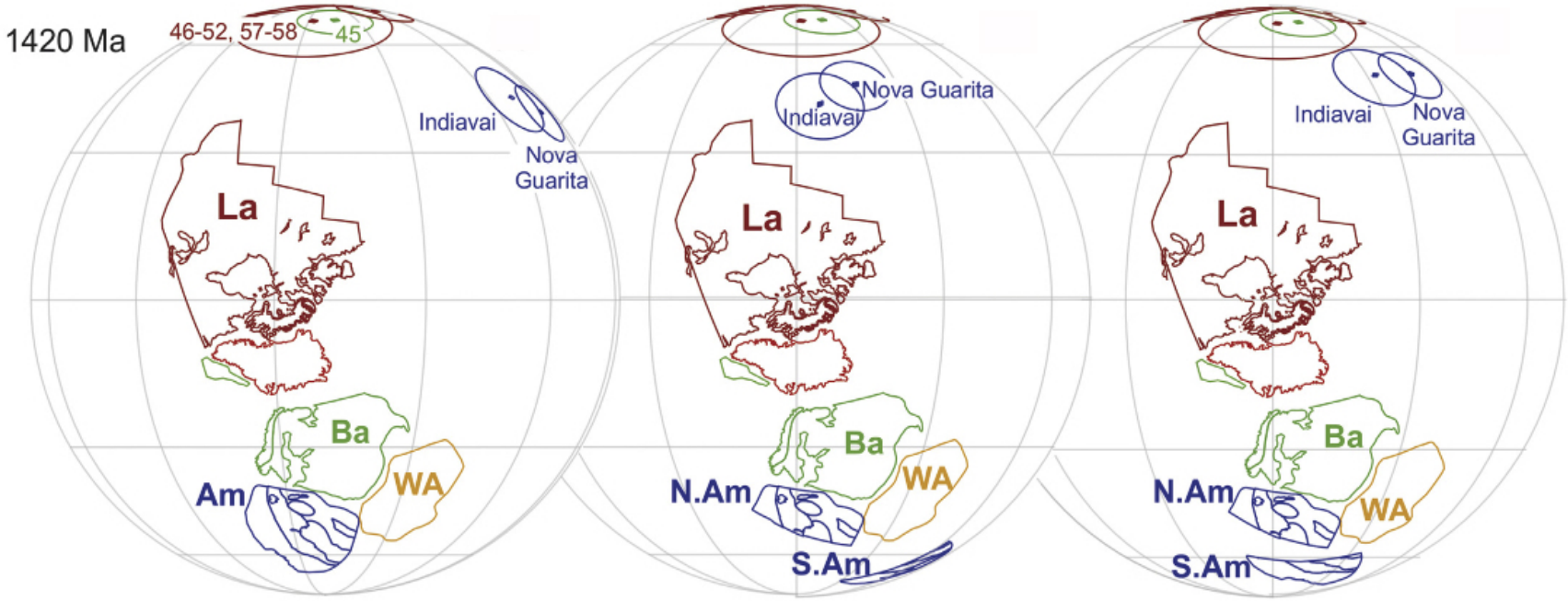
1420 Ma
46-52, 57-58
45
Indiavai
Nova Guarita
La
Ba
Am
WA
N.Am
S.Am

B)

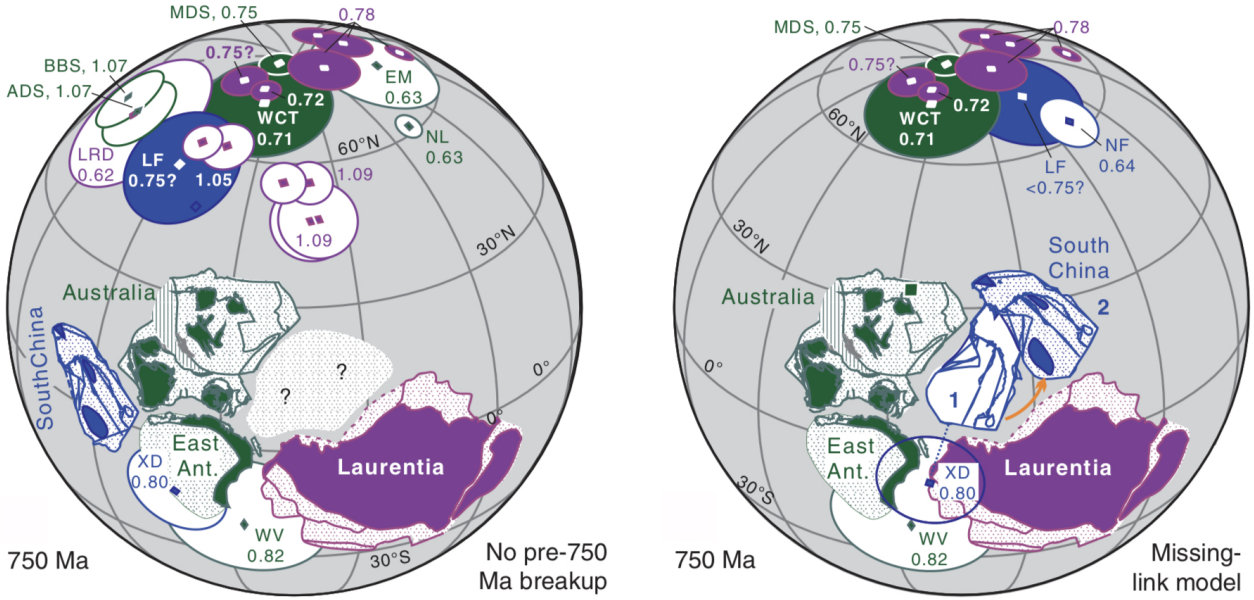
MDS, 0.75
0.78
0.75?
BBS, 1.07
ADS, 1.07
EM
0.63
0.72
WCT
0.71
LRD
0.62
LF
0.75?
1.05
60°N
NL
0.63
1.09
1.09
30°N
Australia
SouthChina
?
?
0°
East
Ant.
XD
0.80
Laurentia
WV
0.82
30°S
750 Ma
No pre-750
Ma breakup
MDS, 0.75
0.78
0.75?
60°N
0.72
WCT
0.71
NF
0.64
LF
<0.75?
30°N
South
China
2
Australia
0°
1
East
Ant.
XD
0.80
Laurentia
30°S
WV
0.82
750 Ma
Missing-
link model

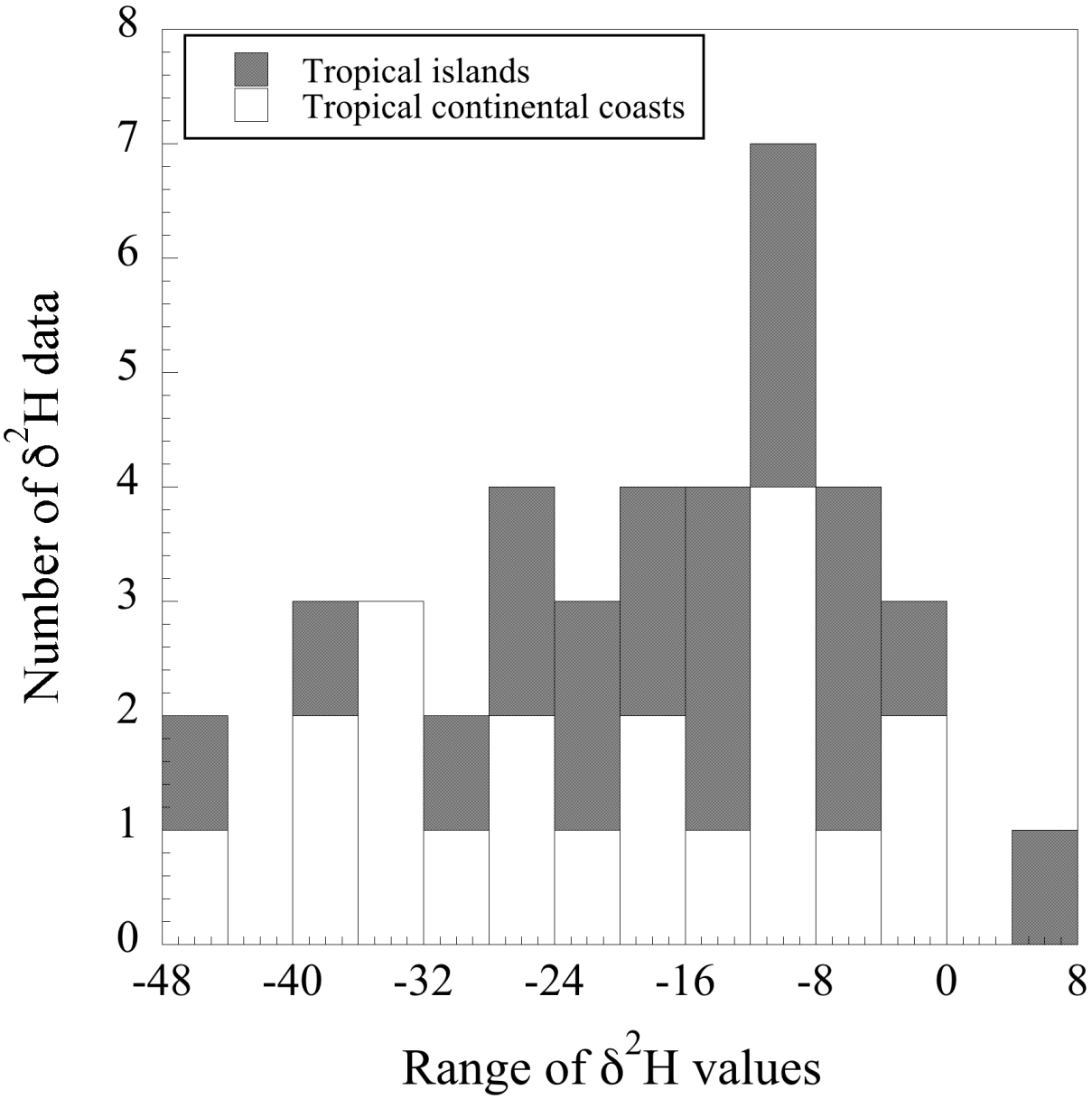
Tropical islands
Tropical continental coasts
Number of δ2H data
Range of δ2H values
0
1
2
3
4
5
6
7
8
-48
-40
-32
-24
-16
-8
0
8

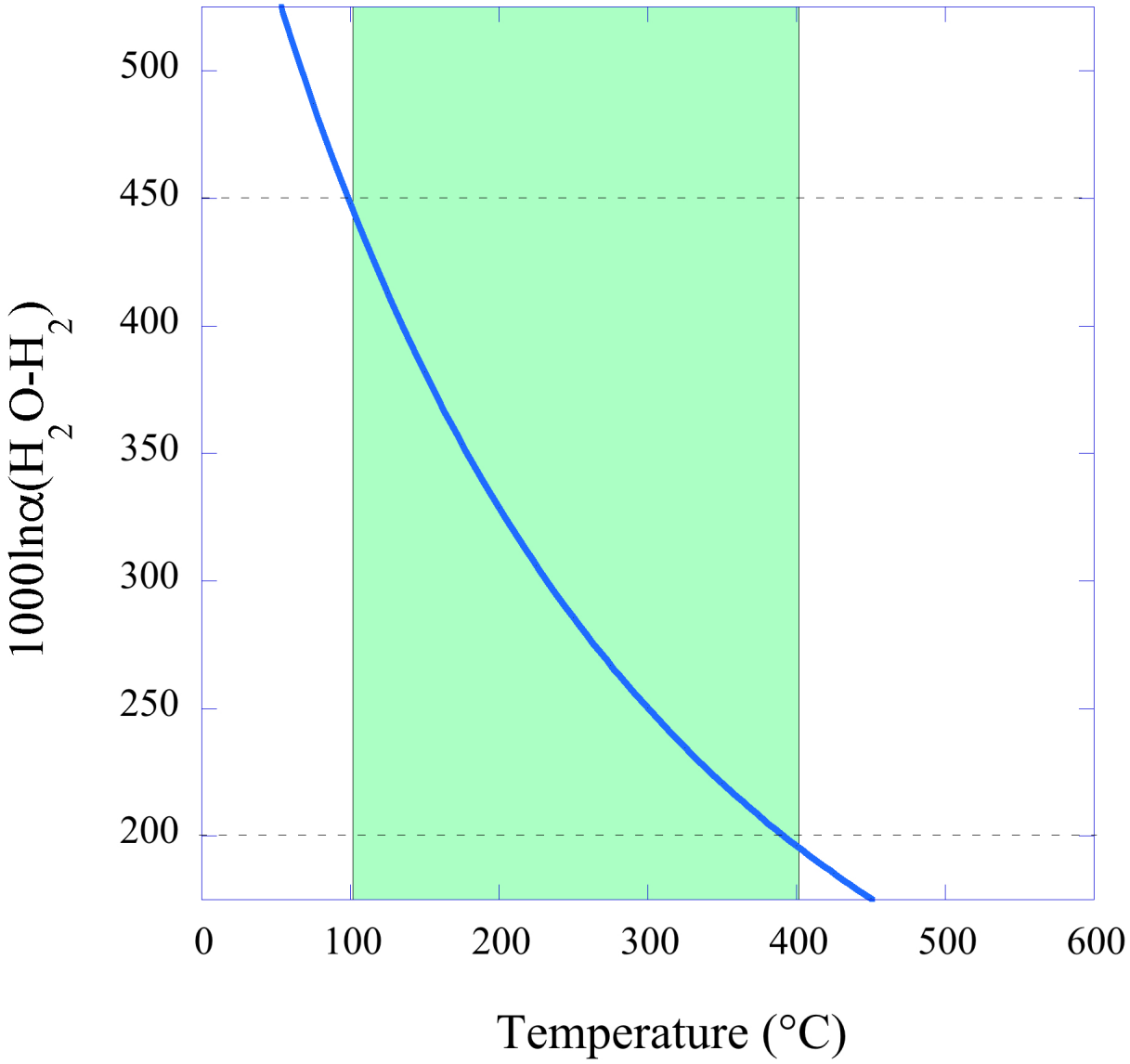
500
450
400
350
300
250
200
1000lnα(H2O-H2)
0
100
200
300
400
500
600
Temperature (°C)

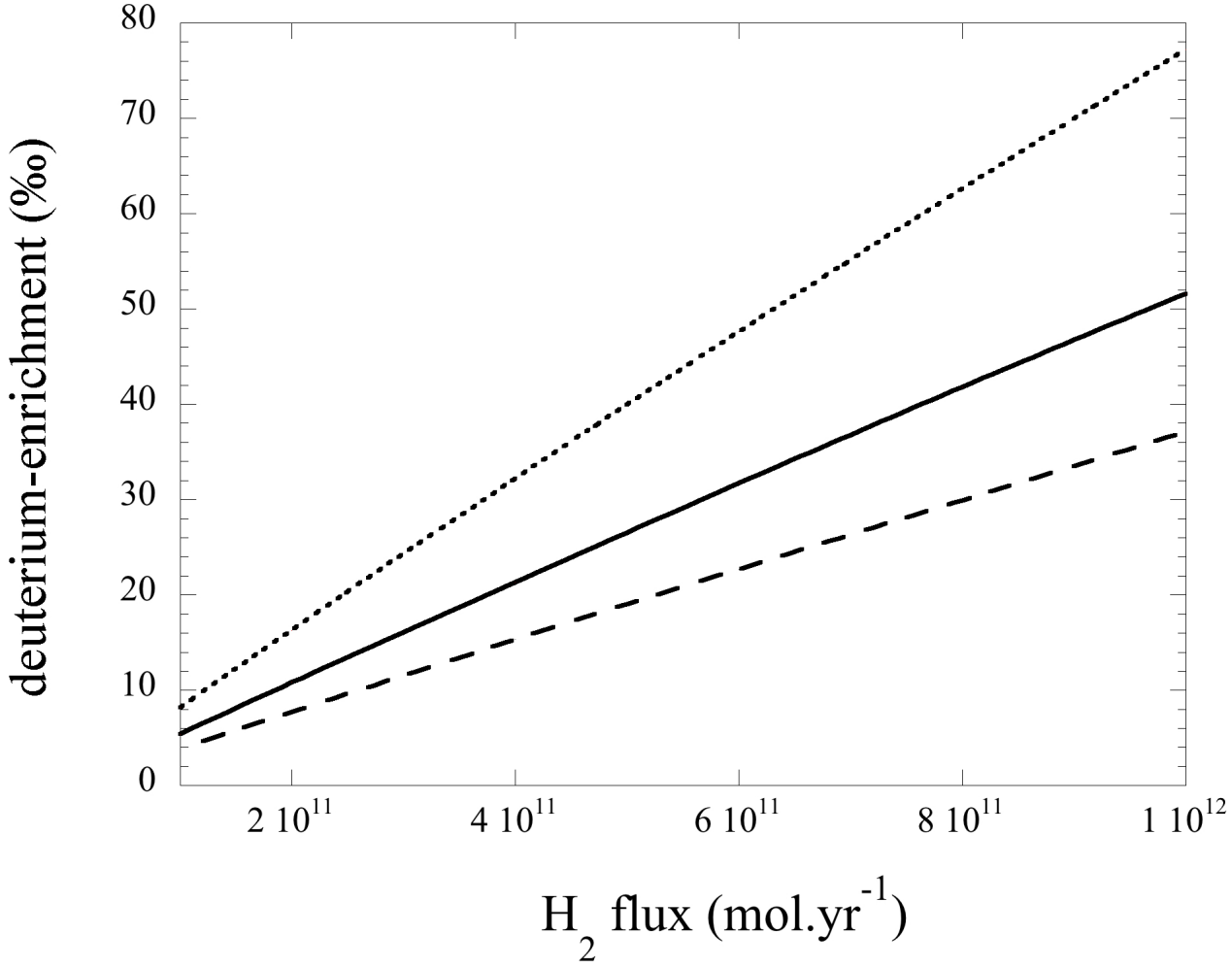
deuterium-enrichment (‰)
80
70
60
50
40
30
20
10
0
2 10^11
4 10^11
6 10^11
8 10^11
1 10^12
H2 flux (mol.yr-1)

Sample	δ^2H	S.D.	N	H (ppm)
Officer Basin, Australia				
L1466	-60.4	6.3	3	93
E1478	-37.6	8.5	4	80
E1482	-70.9	8.8	3	95
E1492	-58.3	6.1	3	324
E1497	-89.1	4.6	4	130
E1502	-54.9	5.3	4	179
Sibley Group, Canada				
P1	-66.2	3.2	4	125
P2	-72.5	5.8	3	44
P3	-57.9	3.6	4	49
P4	-74.1	3.0	4	122
P5	-59.6	7.5	4	65
P6	-59.1	6.7	4	150
P7	-64.9	5.1	3	91
P8	-53.8	2.5	3	186